

**THE CHARACTERISTICS OF THERMAL ENERGY AND MOMENTUM
TRANSFER ACROSS SOLID-LIQUID (S-L) INTERFACES BETWEEN FACE-
CENTERED CUBIC (FCC) LATTICE AND SIMPLE LIQUID**

MOHAMAD DANIAL AIMAN BIN MOHAMAD ZIN



UNIVERSITI TEKNIKAL MALAYSIA MELAKA

2019

DECLARATION

I declare that this project report entitled “The Characteristics Of Thermal Energy And Momentum Transfer Across Solid-Liquid (S-L) Interfaces Between Face-Centered Cubic (Fcc) Latice And Simple Liquid” is the result of my own work except as cited in the references



Signature	:
Name	:
Date	:

اونيورسيتي تيكنيكل مليسيا ملاك

UNIVERSITI TEKNIKAL MALAYSIA MELAKA

APPROVAL

I hereby declare that I have read this project report and in my opinion this report is sufficient in terms of scope and quality for the award of the degree of Bachelor of Mechanical Engineering.

Signature :

Name of Supervisor :

Date :



اونيورسيتي تيكنيكل مليسيا ملاك

UNIVERSITI TEKNIKAL MALAYSIA MELAKA

DEDICATION

To my beloved mother and father



ABSTRACT

The transfer of thermal energy and momentum over the solid-liquid (S-L) interface for alkanes liquid, which are typical liquids applied for lubrication, contacting gold (Au) having the Face-Centered Cubic (FCC) structure with two types of crystal planes, (100) and (111) were examined using Non Equilibrium Molecular Dynamics (NEMD) simulations. The influence of the lattice-scale roughness of the solid surface was determined. Two configurations consists of shear system and non-shear system were made. The non-shear system was applied with constant heat flux and different temperatures between two sides of solid walls and liquid alkanes. The two parallel solid walls sliding at a constant speed and in opposite directions caused viscous heating to occur on the liquid for the shear system. The surface layer of solid atoms and first absorption layer was analysed. There is a temperature jump on the shear and non-shear system where the temperature jump measured for the non-shear system was seen to be larger than the shear system. For the shear system, the slip length was examined. The slip length was found to be affected by the surface roughness. The thermal boundary resistance was measured for both setup to understand the characteristic of thermal energy transfer. It was found that the shear system and surface structure influenced significantly the thermal energy transfer at S-L interfaces.

ABSTRAK

Pemindahan tenaga haba dan momentum ke atas (SL) antara muka pepejal-cecair untuk alkana cecair, yang adalah cecair yang biasa digunakan untuk pelinciran, menghubungi emas (Au) mempunyai padu berpusatkan muka dengan dua jenis pesawat kristal, (100) dan (111) diperiksa dengan menggunakan ketidakseimbangan molekul dinamik simulasi. Pengaruh kekasaran skala kekisi permukaan pepejal telah ditentukan. Dua konfigurasi sistem ricih dan sistem bukan ricih telah dibuat. Sistem bukan ricih telah digunakan dengan fluks haba tetap dan suhu yang berbeza antara kedua-dua belah dinding pepejal dan cecair alkane. Kedua-dua dinding pepejal selari meluncur pada kelajuan yang tetap dan pada arah yang bertentangan, mengakibatkan alkana cecair yang diluncurkan, menyebabkan pemanasan likat berlaku pada cecair untuk sistem ricih. Lapisan permukaan atom pepejal dan lapisan penyerapan pertama cecair telah dianalisis. Terdapat lompatan suhu pada sistem ricih dan bukan ricih di mana lompatan suhu yang telah diukur untuk sistem bukan ricih dilihat lebih besar daripada sistem ricih. Untuk sistem ricih, panjang slip diperiksa. Panjang tergelincir didapati terjejas oleh kekasaran permukaan. Rintangan sempadan termal diukur untuk kedua-dua persediaan bagi memahami ciri-ciri pemindahan tenaga haba. Ia didapati bahawa sistem ricih dan struktur permukaan sangat mempengaruhi pemindahan tenaga haba di antara muka S-L.

ACKNOWLEDGEMENT

In the Name of Allah, the Most Beneficent, the Most Merciful. All praised to the Prophet Muhammad SAW. Firstly, thankful to Allah SWT for gave me this great chance to go through this study and finish it successfully. I am very grateful to Universiti Teknikal Malaysia Melaka (UTeM) for giving me this opportunity to undergo research for my Bachelor of Engineering.

I would like to express my greatest appreciation to my supervisor, Dr Abdul Rafeq Bin Saleman from the Faculty of Engineering at (UTeM) for his outstanding supervision, support, constructive criticism and comments towards the completion of this project. He taught me and showed me a good example of how a PhD-certified lecturer should be.

Also not forgotten my friends for giving me a sum of useful advice. I am deeply thankful to my brother, sister, father and especially my mother for the moral support and encouragement in completing this study. Finally, I would like to thank everyone who had involved in the crucial parts of realization of this study.

TABLE OF CONTENT

CHAPTER	CONTENT	PAGE
	SUPERVISOR'S DECLARATION	
	APPROVAL	
	ABSTRACT	i
	ABSTRAK	ii
	ACKNOWLEDGEMENT	iii
	TABLE OF CONTENT	iv
	LIST OF TABLES	vii
	LIST OF FIGURES	viii
	LIST OF APPENDICES	x
	LIST OF ABBREVIATIONS	xi
CHAPTER 1	INTRODUCTION	
	1.1 Background	1
	1.2 Problem Statement	3
	1.3 Objective	4
	1.4 Scope Of Project	4
CHAPTER 2	LITERARURE REVIEW	
	2.1 Introduction	5
	2.2 Molecular Dynamic Simulation	5
	2.2.1 Simulation System	6
	2.2.2 Potential Function	7
	2.2.2.1 Liquid	7
	2.2.2.2 Solid	9
	2.2.3 Numerical Integration Method	9
	2.2.4 Thermostat and Barostat	10
	2.2.5 Thermodynamic Properties	12

2.2.5.1	Density	12
2.2.5.2	Temperature	12
2.2.6	Slip Length	13
2.2.7	Measurement of Heat Flux	14
2.2.9	Heat Flux and Thermal Boundary Resistance	15
CHAPTER 3	METHODOLOGY	
3.1	Introduction	16
3.2	Simulation system and Potential Functions	16
3.2.1	Simulation System	16
3.2.2	Liquid Alkane	17
3.2.3	Solid of Gold	18
3.3	Boundary Condition	19
3.4	Simulation Detail	20
3.4.1	Numerical Integration Method	22
3.4.2	Barostat and Thermostat	22
3.4.3	Measurement of Structural Quantity	23
3.4.3.1	Density	23
3.4.4	Measurement of Physical Quantity	23
3.4.4.1	Temperature	23
3.4.5	Measurement of Slip Length	24
3.4.6	Measurement of Heat Flux	24
3.4.7	Thermal Boundary Resistance	25
CHAPTER 4	RESULT AND DISCUSSION	
4.1	Introduction	26
4.2	Density	26
4.2.1	Solid walls of (100) and (111) Crystal Plane	26
4.2.2	Liquid methane of (100) and (111) Crystal Plane	28
4.3	Temperature	30
4.2.1	Non-Shear System	30
4.2.2	Shear System	33
4.4	Slip Length	36

4.5	Thermal Boundary Resistance	37
CHAPTER 5 CONCLUSION AND RECOMMENDATION		
5.1	Conclusion	38
5.2	Recommendation	38
REFERENCES		39
APPENDICES		46



LIST OF TABLES

TABLE	TITLE	PAGE
Table 3.1	The size of the simulation system	20
Table 4.1	The slip length for CH ₄ liquid contacting with (100) and (111) crystal plane	37
Table 4.2	The overall results for TBR of non-shear system	37
Table 4.3	The overall results for TBR of shear system.	37



LIST OF FIGURES

FIGURE	TITLE	PAGE
Figure 3.1	The simulation system for the non-shear system	17
Figure 3.2	The simulation system for the shear system setup	17
Figure 3.3	Surface structure of (100) and (111) crystal plane	19
Figure 3.4	Flowchart of the simulation system	21
Figure 4.1	The density distributions of (100) crystal plane	27
Figure 4.2	The density distributions of (111) crystal plane	28
Figure 4.3	Density distribution of liquid methane of (100) and (111) crystal plane.	29
Figure 4.4	Density distribution for (100) and (111) crystal plane.	29
Figure 4.5	Definition of slab for the temperature and velocity distribution for (100) crystal plane	30
Figure 4.6	Temperature distribution of non-shear case for (100) crystal plane	31
Figure 4.7	Temperature distribution of non-shear case for (111) crystal plane	32
Figure 4.8	Temperature distribution of non-shear system for (100) and (111) crystal plane.	32
Figure 4.9	The temperature distribution of non-shear system for the left side of (100) crystal plane.	33
Figure 4.10	Velocity distribution of shear system for (100) and (111) crystal plane	34
Figure 4.11	Temperature distribution of shear system for (100) crystal plane.	35

Figure 4.12	Temperature distribution of shear system for (111) crystal plane.	36
Figure 4.13	The slip length of the right side of (111) crystal plane.	36



LIST OF APPENDICES

APPENDICE	TITLE	PAGE
Table 1.1	Gantt Chart of PSM 1	46
Table 1.2	Gantt Chart of PSM 2	46



LIST OF ABBREVIATIONS

AA	All-Atom
AUA	Anisotropic United Atom
EAM	Embedded Atom Model
FCC	Face-Centered Cubic
HPC	High-performance computing
LJ	Lennard Jones
MBR	Momentum Boundary Resistance
MD	Molecular Dynamic
NEMD	Non Equilibrium Molecular Dynamic
OPLS	Optimized Potentials for Liquid Simulations
PBC	Periodic Boundary Conditions
r-RESPA	Reversible Reference System Propagator Algorithm
RESPA	Reference System Propagator Algorithm
S-L	Solid-Liquid
SKS	Siepmann, Karabomi and Smit
TBR	Thermal Boundary Resistance
TJ	Temperature Jump
TraPPE	The Transferable Potentials for Phase Equilibria
UA	United Atom
VJ	Velocity Jump
VLCC	Vapor-Liquid Coexistence Curves

CHAPTER 1

INTRODUCTION

1.1 Background Information

Technology has advanced a lot in the last few decades. Technology sometimes involves a particular piece of apparatus, however that apparatus are often unbelievably straightforward or dazzlingly complicated. It can be anything from the discovery of the wheel, all the way up to laptops and personal computer. The word technology can be described as the science or knowledge that can be used in practice to solve major or minor problems or to invent useful tools to ease our daily lives. Human have achieved a lot with the aid of technology such as people can still keep in touch with their friends, even though the friend is on the other side of the earth and they have cured many diseases that it had never been cured before.

Tribology is one of the oldest technologies in the world. Tribology literally means “the science of rubbing” based on the dictionary. It can be defined as the science and technology of interacting surfaces in relative motion and of related subjects and practices (Bhushan, 1973). Tribology includes studying and applying the principle of friction, lubrication and wear. The knowledge of various disciplines including physics, chemistry, materials science, solid mechanics, fluid mechanics, applied mathematics, thermodynamics, heat transfer, lubrication, rheology, machine design, reliability and performance are required to understand the surface interaction in a tribological interface which is very complicated (Bhushan, 1973). Numerous of research and study regarding tribology has been done which leads to better performance, fewer breakdowns, greater plant efficiency and significant savings. The main purpose of the research in tribology are mainly to minimalize and eliminate losses resulting from friction and wear at all levels of technology that involve with the rubbing of surfaces (Bhushan, 1973).

Lubrication system, which is a field of Tribology is one of the technology that can clearly be seen in everyday life whether directly or indirectly. The lubrication system is one of the oldest technology in the world. It has been introduced for thousand years ago. Lubrication system is the application of lubricant that reduce the frictional resistance and wear or other forms of surface deterioration between two load-bearing surfaces (Ko, 1985). Initially, lubricants were based on olive oil and rapeseed oil, as well as animal fats. Then,

when the civilization enters the Industrial Revolution, the growth of lubrication accelerated in the Industrial Revolution going along with the use of metal-based machinery (Hsu, 2004). Nowadays, most of the lubrication system are being researched at the molecular scale due to recent development in nanotechnology (A.R. Saleman et al., 2018). Therefore, the study of lubrication at the molecular scale is greatly beneficial for the next generation.

Solid-Liquid (S-L) interface is one of common system in terms of tribology applications for the lubrication system. The typical case for lubrication is when the S-L interface is in the nanometer scale (Abdul Rafeq bin Saleman, Chilukoti, Kikugawa, Shibahara, & Ohara, 2017a). Generally, S-L interface plays an elementary role in numerous fields and the application of the interface is numerous such as batteries, fuel cells, lubricant system or coating system (Streator, 2015). Moreover, S-L interfaces has assists human in various way especially in the industry field. The S-L interface helps with an understanding of the physical phenomena and structural information of the interface, at the atomic scale, for instance in chemical change which is called catalysis, crystal growth, lubrication, chemistry, mixture system, and in several biological reactions (Park & Seo, 2011). In the lubrication system, due to viscous heating, the thermal energy occur from the flow energy in the sheared liquid film. The flow energy, which is a Couette-like macroscopic flow are generated in the sheared liquid film when there is a shear on the two solid surface contacting the liquid with different velocity. Then, the thermal energy increased the temperature of the liquid film and via heat conduction, the increased temperature is transferred over the S-L interface to the solid walls (Abdul Rafeq bin Saleman et al., 2017a). Hence, a good understanding of thermal energy transfer and momentum transfer is important to S-L interfaces and lubrication system.

S-L interface have been frequently studied in order to understand the characteristics of some application. Interfacial thermal resistance is defined as the measurement of thermal resistance between two different surfaces in contact with each other resulting in discontinuity of temperature or drop of temperature at the interface under a heat flux. Numerous of research have been studied regarding the thermal energy transfer and momentum transfer of S-L interface. One of the study that have been done recently are the comparison of the heat transport at S-L interfaces between non-shear and shear (Rafeq et al., 2018). A molecular dynamics simulation, was used for the simulation and the heat flux was measured which were used to determine the thermal boundary resistance (TBR).

For the application like lubrication system, it is important to understand and study the S-L interface that one may give the system more efficient for the future. There are

numerous of research regarding the thermal energy transfer and momentum transfer of S-L interface has been done and explored, but the characteristic of the thermal energy transfer and momentum transfer have not been clearly study. Rafeq (Abdul Rafeq bin Saleman et al., 2017a) has done the investigation of the transfer of thermal energy and momentum over the S-L interface between gold and sheared liquid alkanes. However, the research does not compare between sheared and non-sheared system. Another studies regarding thermal transport has been made by Rafeq (Abdul Rafeq bin Saleman, Chilukoti, Kikugawa, Shibahara, & Ohara, 2017b). The study was on a molecular dynamics study on the thermal transport properties and the structure of the solid–liquid interfaces between Face-Centered Cubic (FCC) crystal planes of gold in contact with linear alkane liquids. The study examined the influences of the lattice-scale roughness of the solid surface in contact with the liquid but it is only based on the thermal transport and the momentum transfer was not considered. The lattice-scale roughness of solid surface in terms of the characteristic of thermal energy and momentum transfer with shear system and non-shear system have yet to be clarify.

Furthermore, Rafeq (Rafeq et al., 2018) have investigated the comparison of the heat transport at S-L interfaces between non-shear and shear systems. From his study, the heat transport characteristics at S-L interfaces were found to be significantly influenced by the shear system and solid wall surface structure. However, the study only focus on the heat transport, while the momentum transfer was not considered.

1.2 Problem Statement

It is crucial to know characteristic and the influences of thermal energy and momentum transfer in order to know which material is better in providing a better lubricant for a better future. This project will study the characteristic and the influences of thermal energy and momentum transfer across the S-L interface. The transfer of thermal energy and momentum over the S-L interface for alkanes liquid, which are typical liquids applied for lubrication, contacting gold (Au) having the Face-Centered Cubic (FCC) structure with two types of crystal planes, (100) and (111). The influence of the lattice-scale roughness of the solid surface on thermal energy and momentum transfers at the S-L interface will be examined using Non Equilibrium Molecular Dynamics (NEMD) simulations.

1.3 Objective

Therefore, based on the problem statement which have been describe above, the objective of this research is:

- To identify the characteristics of the transfer of thermal energy and momentum over the solid-liquid interface for simple liquid.
- To clarify the influences of the lattice-scale roughness of solid surface on the characteristics of thermal energy and momentum transfer.

1.4 Scope

The scopes are identified based on the objectives of this research. The 2 Face-Centered Cubic structure with two types of crystal plane which is (100) and (111) will be used in this study. A single liquid alkane (methane) or simple liquid is chosen. The simple liquid are linear liquid and not lengthy molecule. The thin liquid is sandwiched between two parallel solid walls where the liquid alkane is put between two solid walls which is gold (Au). The factor that will be measured in this research on the S-L interface are density, temperature, heat flux, slip length and the thermal boundary resistance. A Non Equilibrium Molecular Dynamics simulation will be used in this study. The Reversible Reference System Propagator Algorithm (r-RESPA) method with multiple time steps will be used. Two setup of simulation will be made in this study that is non-shear system that and shear system. The non-shear system consists of different temperature; both side of the solid wall are set at low temperature while the liquid at the center is set at high temperature while for the shear system, a constant speed is applied for both of the solid wall in the opposite direction.

CHAPTER 2

LITERATURE REVIEW

2.1 Introduction

This chapter illustrates the literature review from the past about the S-L interface in details. It consists of the criteria that need to be added in studying the characteristic in terms of thermal energy transfer and momentum transfer such as molecular dynamic simulation, simulation model system, the potential function, the thermodynamics properties and measurement method for density, temperature, momentum and heat flux and thermal boundary resistance and momentum boundary resistance.

2.2 Molecular Dynamic Simulation

Molecular Dynamic (MD) simulation is a technique for calculating the equilibrium and transport properties of particle systems. The first simulation was in the 1960s where the model molecules represented by a continuous potential were carried out using MD. In 1964, Rahman (A., 1964) was the first one who calculated the diffusion coefficient in a argon atoms system interacting through a Lennard-Jones potential using MD (Ewen, Heyes, & Dini, 2018).

It is stated that molecular dynamic serves two roles. First, the solutions of the equations of motion for times comparable with the correlation times of interest need to be essentially exact, so that we may accurately calculate time correlation functions. Second, the use the method to generate states sampled from the microcanonical ensemble (Tildesley, n.d.). An ensemble is commonly a probability distribution for the state of the system (Ewen et al., 2018). The microcanonical also called NVE ensemble due to the total number of particles, N , the volume of the system, V and the total energy in the system, E , remain constant.

The Non-Equilibrium Molecular Dynamics (NEMD) simulation is based on time-reversible equations of motion (Wm.G.Hoover, 2005). The first NEMD simulation were perform in 1970s which imposed shear flows at large shear rates. Until 1970s, NEMD simulations were quasi-2D where they used periodic boundary conditions (PBC) in only two

directions. Then, equations of motion for imposing shear flow in system which PBC in all three Cartesian direction were created in 1980 (Ewen et al., 2018).

A number of facet must be have been thought about carefully, from the inherent limitation of the time and length scales that can be modelled to the accuracy of the representation of the intramolecular and intermolecular interactions in order for NEMD simulation to be useful in terms of predictive capabilities (Ewen et al., 2018). The computer hardware and software available, the system size, as well as the complexity of the force-fields used are the factors that will decide the computational time required to conduct MD simulations.

Classical MD force-fields require a time step of approximately 1 femto second (fs) to ensure energy conservation (Tildesley, n.d.). This means that even when performed on multiprocessor high-performance computing (HPC) systems using highly parallel MD software, only ns or μ s time scales can be accessed in MD simulations in extreme cases, since they correspond to millions / billion timescales (Ewen et al., 2018). The main consequence of the short accessible time scales in NEMD simulations where shear is applied is that relatively high shear rates are required to ensure that the properties of interest reach a stable state (generally $> 10^7 s^{-1}$) (Bair, McCabe, & Cummings, 2002; Bair, McCabe, McCabe, Cummings, & Cummings, 2002). The ability to simulate lower shear rates was a long-term objective of NEMD simulations to facilitate direct overlap with experiments and real components (Ewen et al., 2018).

2.2.1 Simulation System

In MD simulation, there are several simulation system that have been used to study the S-L interface. Numerous of numbers have been studied for the system that consists of a liquid film confined between two parallel solid walls (Khare, Koblinski, & Yethiraj, 2006; Taku Ohara & Torii, 2005; Rafeq et al., 2018; Abdul Rafeq bin Saleman et al., 2017a, 2017b; Soong, Yen, & Tzeng, 2007; Torii, Taku Ohara, & Kenji Ishida, 2007). One of the study used this simulation system to clarify the influence of interaction between solid and liquid molecules and the spacing of molecular alignment on the surface of the solid wall (Torii et al., 2007). It is found that in order to analyse thermal energy flux across the system, many research set the temperature of the left solid wall higher than the right one which it can produce thermal energy flux (Abdul Rafeq bin Saleman et al., 2017b).

Another study has been made on same simulation system on comparing the shear and non-shear system (Rafeq et al., 2018). In the study, two setup have been made to compare the non-shear and shear system, that is the center of the liquid was set at high temperature while both of the solid walls was set at low temperature which is for the non-shear system and for the shear system, a shear was applied on both solid walls with the same speed in the opposite direction with the different temperature setup that was applied on the non-shear system simultaneously. There were numbers of studies that used the shear system at S-L interface to examine the momentum transfer that used the same simulation system (Khare et al., 2006; Taku Ohara & Torii, 2005; Abdul Rafeq bin Saleman et al., 2017a). By using the simulation system that have been describe above, it is observed that the simulation system helps to analyse on the momentum transfer clearly.

2.2.2 Potential Function

Potential function is one of the important factor before starting the simulation. In general, the potential energy is described by pair potentials. The potential energy is usually described by pair potentials. The potential energy contains the interesting information regarding intermolecular interactions. The predictions made by using either analytical equations of state or molecular simulation are only as accurate as the underlying models they employ (Eggimann, Siepmann, & Fried, 2007). Models that make use of transferable parameters are one option for supplementing the low levels of experimental data available for high temperature or high pressure systems. For example, the similar parameter are fitted to be accurate at several state points, including those beyond constraints of the initial parameterization conditions. In general, the potential energy is described by pair potentials.

2.2.2.1 Liquid

In the past, there were three types of common model used to replicate linear alkane liquid namely the united atom (UA) model, the anisotropic united atom (AUA) model and the all-atom (AA) model. The UA model is a good approximation for simulating molecular systems in which the intermolecular motion is much more important than the intramolecular motion. In addition, the UA model was utilized in most recent simulation system where carbon and hydrogen atoms were gathered in as a single interaction site represented as a pseudoatom (Marcus G. Martin and J. Ilja Siepmann, 1998; Taku Ohara, Yuan, Torii, Kikugawa, & Kosugi, 2011; Rafeq et al., 2018; Abdul Rafeq bin Saleman et al., 2017b,

2017a). The UA model are found to be useful for a quantitative understanding of the dynamic behaviour of medium sized alkanes (Mondello & Grest, 1995). Furthermore, UA model capable of quantitatively predicting the adsorption properties of both linear and branched alkanes responsible for neutral molecular sieves (Dubbeldam et al., 2004). The AA model replicates all the atoms in a molecule that made the computation time in a simulation is longer. Every atom is regarded as an individual interaction site in AA model (Guevara-Carrion, Hasse, & Vrabec, 2012). In the AUA model, hydrogen and carbon atoms are grouped in a single interaction site, but a certain distance from the carbon atom is displaced at the center of the force to better account for the presence of the hydrogen atoms (Ungerer et al., 2000).

Marcus (Marcus G. Martin and J. Ilja Siepmann, 1998) stated that there are three united-atom force field; optimized potentials for liquid simulations (OPLS), Siepmann, Karabomi and Smit (SKS) and The Transferable Potentials for Phase Equilibria (TraPPE). The OPLS united atom model was parametrized using isobaric – isothermal Monte Carlo simulations to provide accurate liquid density vaporization heats for short alkanes at atmospheric pressure (Jorgensen & Swenson, 1984). It contains different LJ parameters for the methyl group in ethane, the methyl group in all other n-alkanes and the methylene group. For SKS, Monte Carlo in the Gibbs ensemble was subsequently used to calculate the vapor-liquid coexistence curves (VLCC) of n-alkanes. It used the same LJ diameter, but different magnitude if well depth, to account for methyl and methylene group. Previous study has found that OPLS force-field overestimate the critical temperature of n-alkanes and SKS force-field overestimated the critical temperature of the shorter n-alkanes. The researcher stated that TraPPE models have been shown to be reasonably accurate for several systems beyond the state points and molecules used in the parameter fitting (Eggimann et al., 2007). Molecular interactions in the TraPPE force-field using UA model are described by pairwise-additive Lennard-Jones (LJ) and Coulomb potentials for the non-bonded interactions.

Based on previous studies, most of the investigation use a similar model system regarding to the model systems. For the CH_4 liquid, the UA model are used as the model where carbon and hydrogen atoms were assembled in as a single interaction site represented as a pseudoatom that has been mentioned on the above. It was then modelled by using Transferable Potential for Phase Equilibria (TraPPE) force field (Abdul Rafeq bin Saleman et al., 2017a).

2.2.2.2 Solid

As for the solid walls, there are three common potential function used to replicate metal solid, namely Morse potential, Lennard Jones (LJ) potential and embedded atom model (EAM). For LJ potential, it is the most commonly used interaction model. An attempt was made to parameterize the potential of LJ for metals but no practical application has been found.

The EAM is a many-body potential used for a wider range of metals. Numbers of study has used the EAM model in their research. One of the earlier studies showed that the EAM model provides a good description of gold (Au), copper (Cu), palladium (Pd), silver (Ag), platinum (Pt), nickel (Ni), aluminium (Al) and some of the alloys (Foiles, Baskes, & Daw, 1986). A Morse potential was first proposed by Philip M. Morse in 1929 (Morse Philip M., 1929). Moreover, it was popular potential for simulation of metals that have face centered-cubic and hexagonal close packed structures and it can also be used to study the atomic properties of metals (Girifalco & Weizer, 1959). Similar to Lennard-Jones, but more bonding and better suited for cases where attractive interaction results from the formation of a chemical bond (Zhigilei, 2013).

2.2.3 Numerical Integration Method

It is obvious that a good algorithm to integrate Newton's equation of motion is required for a better MD simulation. The process of integrating the equation of motion can be achieved by using several kinds of algorithm. In the MD simulation, the Newtonian equation of motion decide the movement of the atoms included in molecules. The speed of an algorithm is not really significant due to the small fraction of time spent on integrating the equation of motion. The accuracy of the large time step is more important because the longer the time step, the less force evaluation per unit of simulation time is required. Therefore, it is advantageous to use a sophisticated algorithm that use a long time step (Daan Frenkel; Berend Smit, 1996).

A variety of techniques were introduced to increase the time in molecular dynamic simulations in an attempt to overcome these difficulties. According to Benedict J. Leimkuhler (Leimkuhler, Reich, & Skeel, 1996), there are four categories consists of the numerical integration methods that can be describe based on their way of handling the components of linearized dynamics. The first method are the method that accurately resolve the highest

frequencies. This method can be relate to the explicit method including multiple time stepping and the method LIN (M. Zhang & Skeel, 1997).

In molecular dynamics, the most commonly used time integration algorithm is probably the so-called Verlet algorithm (Daan Frenkel; Berend Smit, 1996). This algorithm is simultaneously simple to implement, accurate and stable, explaining its great popularity among simulators of molecular dynamics. Over the years this integrator has undergone various extensions and modification. A MD simulations are carried out using the velocity Verlet algorithm.

Moreover, the reference system propagator algorithm (RESPA) used to generate efficient reversible and symplectic integrators for systems with long and short distance forces and for systems in which the degrees of freedom can be divided into fast and slow subsets (Berne, 1999). Multiple time step methods, such as the reversible reference system propagator algorithm (rRESPA), enable the slowly varying system components to be integrated with a rather long time step while still using smaller time steps for the fastest moving components. (Stuart, Zhou, & Berne, 1996). Different implementations of the rRESPA method have been applied to a wide range of systems, leading to speeds of 4 to 15 factors.

2.2.4 Thermostat and Barostat

For the simulation system to achieve the suitable state, the temperature and pressure of the system need to be maintain at certain values. Due to that, the thermostat and barostat will help the system to achieve that suitable state. Several extensions of the MD method have been proposed to apply MD simulations in various situations. The constant temperature or pressure methods are typical extensions that under constant temperature or pressure conditions perform MD simulations. One of the purpose of using thermostat in MD are to match experimental condition. An instantaneous temperature is required for the use of thermostat. Generally, the methods for temperature control can be classified into several types, which are the constraint method, the extended system method and the stochastic method (Shuichi Nose, 1991). Among these types, there are many famous methods of applying thermostat to control or maintain the temperature, such as the Woodcock's velocity-scaling method, Gaussian constraint method, Nose-Hoover extended system method (HOOVER, 1985) and stochastic method (Andersen, 1980).

The stochastic method, the method that kept the temperature at a constant value by the balance between thermal agitation due to the random force and slowing down due to friction (Shuichi Nose, 1991). One of the stochastic method are Anderson thermostat (Andersen, 1980). It was developed by Anderson himself in 1980 that the velocity was modified by using stochastic forces to maintain average kinetic energy of the molecular system consistent with the equipartition theorem. The Nose-Hoover thermostat of extended system method, was first suggested by Nose (S. Nose, 2002; Shuichi Nose, 1984) and later modified by Hoover (HOOVER, 1985). It affects the intermolecular force from extended ensemble system which generates canonical temperature fluctuations.

In the Gaussian constraint method, the constant temperature condition is achieved by suppressing the kinetic energy's thermal fluctuations and maintaining it at a constant value (Shuichi Nose, 1991). This type of method in classical dynamics is classified as the non-holonomic case, where the method applied on molecular dynamics is discussed by Haile and Gupta. In addition, Evans (Evans, 1983) proposed the Gaussian thermostat from the formulations in the NEMD simulations. He conclude that the actual constrained motion should occur along a trajectory obtained by normal projection of a force onto a constraint hypersurface.

Velocity-scaling method by Woodcock's is the earliest method of simulation at constant temperature. It was a simple algorithm to maintain total kinetic energy to a constant value was proposed by Woodcock in 1971 (Woodcock, 1971). It is proved that Woodcock's velocity scaling scheme in the Verlet algorithm is close to the Gaussian thermostat (Shuichi Nose, 1991). Numbers of studied has used velocity-scaling method to maintain their temperature.

In term of constant pressure, to control the pressure, volume change or work transfer should be allowed (Shuichi Nose, 1991). It is stated that the common methods for barostat are Berendsen barostat, Andersen barostat and Parrinello-Rahman barostat (Ruhle, 2008). For the Berendsen barostat (Berendsen, Postma, Van Gunsteren, Dinola, & Haak, 1984), the system is weakly coupled to an external bath by the principle of the least local perturbation. The Andersen method (Andersen, 1980) for adjusting the pressure in a simulation was developed Particles interacting. The method was later extended by Parrinello to anisotropic coupling and Nose to molecular systems. In Parrinello-Rahman barostat (Parrinello & Rahman, 1981), Parinello and Rahman extended Andersen's method, allowing the simulation box to change its shape as well.

2.2.5 Thermodynamic Properties Measurement

2.2.5.1 Density

Density distribution in a simulation system gives an insight into the liquid condition. The previous study indicated that the simulation system density distributions were obtained by dividing rectangular slabs with a thickness of 0.02 \AA in z-direction, where the thickness used are constant. Each slab has their own density where the density was measured based on the number of molecules for CH_4 liquid. After the density has been measured, the density profile between CH_4 and both side of solid wall can be done. It is found that the shear applied on the liquid does not affect the density distribution where the density distribution from non-shear and shear system are alike. (Khare et al., 2006; Abdul Rafeq bin Saleman et al., 2017a).

The previous study shows the density distribution of the liquid oscillate near the solid walls and the peak represents the adsorption layers of liquid molecules on the solid surface. The absorption layer of liquid molecules that contact with solid wall surface are referred as the first absorption layer. The density of solid atoms in the surface layer influence the packing density of the liquid molecules in the first adsorption layer. The surface layer of the solid atoms is stated as the layer of solid atom that are closest to the liquid film. From the observation of the past study, Rafeq (Abdul Rafeq bin Saleman et al., 2017a) affirm that the surface layer of solid atom is significantly influenced the first absorption layer of liquid.

2.2.5.2 Temperature

Temperature is one of the basic physics concepts. It is one of the way to identify the characteristic of thermal transfer in most of the situation. From the past study, different slab thicknesses were used in the temperature profile because the thickness of the absorption layer for the liquid differs between each layer, types of crystal planes and types of alkanes. (Abdul Rafeq bin Saleman et al., 2017a) The system was divided into a number of slabs in order to calculate the local temperature in the system. The purpose of dividing line between each slab are used as a control surface to measure the average heat flux of the system. The temperature of the system was calculated from the kinetic energy corresponding to the random component of velocity for each pseudoatoms which were located in the slab. Below are the velocity distribution and temperature distribution for the case of CH_4 liquid contacting based on the previous researched. (Abdul Rafeq bin Saleman et al., 2017a) Temperature is determined for systems with fluid flow by using the kinetic energy calculated

based only on the “specific” or “thermal” part of the atom velocity where it is obtained by subtracting the net local flow velocity from the total velocity of the atoms (Khare et al., 2006).

In addition, the appearance of the temperature jump (TJ) at the solid-liquid interfaces was also reported in the literature (Barisik & Beskok, 2014; Torii, Ohara, & Ishida, 2010) and a phonon mismatch at the interface was explained to be the reason. (Swartz & Pohl, 1989) From past study, the measurement method to measure the TJ is the temperature distribution of solid walls at first are fit to a linear line and the temperature distribution of liquid alkanes are fit to a quadratic line. The two lines were then extrapolated to the midpoint of the equilibrium positions of the solid atom surface layer and the first absorption layer of liquid molecules. Next, the temperature difference between the solid and liquid were determined (Abdul Rafeq bin Saleman et al., 2017a, 2017b). As a result, it can be conclude that a small TJ can be found when the shear rate and viscous heating generated in the liquid is small. The similar method was used to determine velocity jump (VJ) at the S-L interface, but the velocity distributions of liquid alkanes were fit to a linear line (Abdul Rafeq bin Saleman et al., 2017a). A velocity distribution curve for the Couette-like flow of liquid was approximated by a polynomial equation, and the flow velocity of the liquid at the S-L interface was extrapolated using this equation to define the VJ at the S-L interface (Taku Ohara & Torii, 2005).

2.2.6 Slip Length

The slip length is defined as the linearly extrapolated velocity of liquid from the S-L interface into the solid walls, where the tangential velocity of liquid coincides with the velocity of solid walls. The response of the slip length to the length of the molecular chain of liquids was first reported by Khare (Khare et al., 2006) where he examined the linear alkane liquids in contact with model wall, which is a single layer of solid atom attached to a FCC sites. The previous study indicates that the slip length is correlated with the length of molecular chain for liquids and surface structure of solid walls (Abdul Rafeq bin Saleman et al., 2017a). The surface structure of the solid walls was claimed to affect the slip near the S-L interface.

2.2.7 Measurement of Heat Flux

In order to understand the characteristic of thermal energy, heat flux is considered to be the most crucial quantity in thermophysical engineering (Torii, Nakano, & Ohara, 2008). Heat flux can be measure by using the equation derived by Irving-Kirkwood (Taku Ohara, 1999a; Yang, Wu, & Li, 2012). The equation derived by Irving and Kirkwood however, is only valid for pair potentials such as the LJ, and does not apply to systems with many-body potential, which are usually included in molecular models for diamond structured materials or organic compounds and biomolecules (Torii et al., 2008). Due to that, there are several method that have solved this, Zhang and Todd (J. Zhang & Todd, 2004) proposed a formula for calculating the heat flux vector with a contribution of a many-body potential included. It is found that their method has the advantage when the system is non-uniform where Irving-Kirkwood formula declared the difficulties in treating the different temperature.

Another work was done by Chen, whose expression is for a local heat flux vector instead of a spatial one. Chen followed Hardy's idea and formulation method and extended it to three-body potential types Tersoff and Stillinger-Weber. In 2008, the molecular dynamic expression heat flux involving many-body potential was derived by Torii and Ohara (Torii et al., 2008). The concept of intermolecular energy transfer, previously proposed by the authors, was extended as the dominant element of heat conduction in dense liquids, the energy transfer between sites for which a multi- body potential was defined.

From the recent study, an instantaneous heat flux can be achieved by changing the expression assuming uniformity of the system and no macroscopic fluid flow. Rafeq (Abdul Rafeq bin Saleman et al., 2017a) asserted that the heat flux consist of two terms. The first term illustrates the kinetic and potential energy of molecules and the second term portray the transfer of intermolecular energy due to intermolecular forces between molecules (Abdul Rafeq bin Saleman et al., 2017a). In the past study, by dividing the line between each slab can be used as a control surface, which the average heat flux across the system can be measured (Abdul Rafeq bin Saleman et al., 2017a). Furthermore, the heat flux can be measured with a control surface or control volume that was performed by previous authors (Torii et al., 2008). Both equations of control surface and control volume have similar forms. The measurement method is the difference between the two equations. The measurement for equation across control surface is measured at a control surface (T. Ohara & Suzuki, 2000; Abdul Rafeq bin Saleman et al., 2017a), while the heat flux across control volume gives the average heat flux across the direction of the heat flux (Taku Ohara, 1999a).

2.2.8 Thermal Boundary Resistance

Viscous heating was found due to the sheared of the liquid which leads to heat conduction from the liquid to the solid via the S-L interfaces. (Abdul Rafeq bin Saleman et al., 2017a). The Thermal Boundary Resistance (TBR) at the interface can be determined using the direct method from heat flux and temperature jump in order to understand the characteristic of thermal energy at S-L interface (Landry & Mcgaughey, 2009). The equation to calculate TBR are shown below (Barisik & Beskok, 2014; Rafeq et al., 2018; Abdul Rafeq bin Saleman et al., 2017a, 2017b):

$$\text{TBR} = \frac{\Delta T}{J} \quad (2.2)$$

From the equation above, ΔT represents temperature jump at the interface between the solid wall and the liquid which was obtained by the procedure, while J represent the heat flux across the interface. It is known from past studies, The TBR at the S- L interface is correlated with the gap distance and lattice-scale structure of solids, depending on the length of the liquid molecular chain (Abdul Rafeq bin Saleman et al., 2017a). The molecular length of liquids and correlated with the distance between the contacting layers of solid and liquid affects the TBR at the S-L interfaces. One of the previous study (Abdul Rafeq bin Saleman et al., 2017a) found that the contribution of thermal energy transfer in x - and y - components is therefore the influence of the surface structure of solid walls due to the lattice scale corrugation occur at the (110) crystal plane, also reported in other studies (Taku Ohara & Torii, 2005; Torii et al., 2010). Furthermore, with it is understood that sheared liquid influences the characteristics of heat transport at S-L interface with the TBR (Rafeq et al., 2018).

CHAPTER 3

METHODOLOGY

3.1 Introduction

In methodology, computational method applied for this study will be shown. Generally, this study concern the analysis of characteristic of thermal and momentum energy transfer across FCC lattice and liquid alkane by using Non Equilibrium Molecular Dynamics (NEMD) simulation. The reason of using NEMD simulation is because the simulation correspond more closely to the experimental procedure. The molecular-scale could not be predicted or easily determined based on the conventional macroscopic concepts because of their unusual characteristics. The topic that will be cover are the simulation system, potential functions, boundary condition and simulation detail.

3.2 Simulation System and Potential Functions

3.2.1 Simulation System

The simulation system consists of a liquid film confined between two parallel solid walls. For this study, both of the solid walls consist of FCC crystal of gold (Au) with three type crystal of crystal plane which is (100) and (111). The liquid film consist of a single species of alkane that is, methane (CH_4). The system of liquid film confined between two parallel solid walls has been utilized in many studies that have been shown at Chapter 2. Because of that, a similar model is will be used for the simulation system. There are two setup of simulation system will be studied in this project which are the system for the thermal energy transfer between two stationary solid walls and the system for the thermal energy and momentum transfer that happen simultaneously between the solid walls moving in an opposite direction with the same speed. Figure 3.1 and Figure 3.2 shows the simulation system for non-shear and shear system consisting of liquid sandwiched between two solid parallel walls.

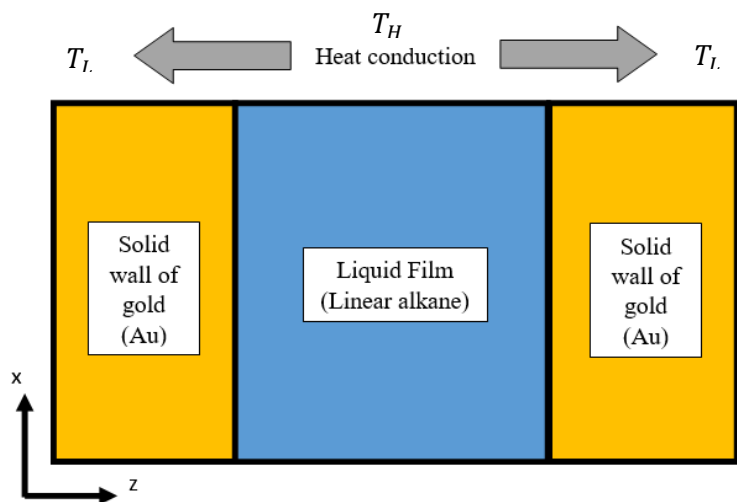


Figure 3.1: The simulation system for the non-shear where the heat conduction occur due to high temperature to the low temperature.

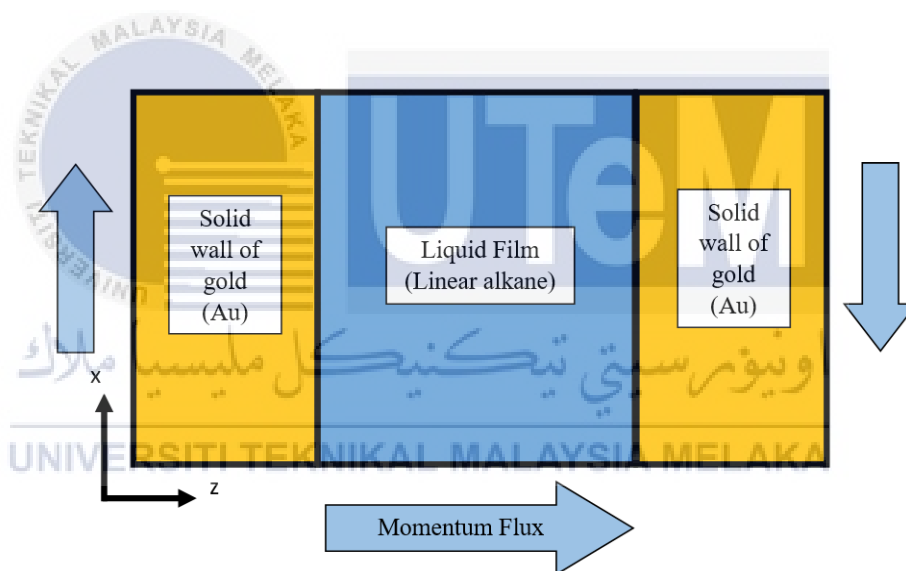


Figure 3.2: The simulation system for the shear system setup. The shear is applied at the both side of solid walls with a constant speed in the opposite direction.

3.2.2 Liquid Alkane

In MD simulation, the liquid and solid of the system are replicated based on the potential function and model where the model represents molecule or atom and the potential function represent the interaction between molecules or atoms. The CH_4 liquid that consist of hydrogen and carbon will be modelled using the united-atom (UA) model which have been describe in the Chapter 2 where all the atoms in a CH_4 group are treated as a single pseudo-atom. The UA model is chosen because the force fields significantly reduce the

number of atoms for which non-bonded interactions must be calculated, thus reducing the computational cost by an order of magnitude. (Marcus G. Martin and J. Ilja Siepmann, 1998) This has made them very popular in tribology, which often requires simulation of large multi-component systems. For the potential function, the LJ 12-6 potential will be used, (Abdul Rafeq bin Saleman et al., 2017a, 2017b) which are:

$$U^{LJ}(r_{ij}) = 4 \varepsilon_{ij} \left[\left(\frac{\sigma_{ij}}{r_{ij}} \right)^{12} - \left(\frac{\sigma_{ij}}{r_{ij}} \right)^6 \right], \quad (3.1)$$

(1)

where r_{ij} is the distance between atoms i and j . The molecular interaction between the pseudoatoms was considered using LJ potential, where the $\varepsilon_{CH_4} = 2.0433 \times 10^{-21}$ J and $\sigma_{CH_4} = 3.73 \text{ \AA}$ based on Transferable Potential for Phase Equilibria (TraPPE) force fields which the force field have been shown to be reasonably accurate for several systems beyond the state points and molecules used in the parameter fitting. For the interaction between two different type of pseudoatoms or molecules, the parameter are calculate using the standard Lorentz-Berthelot combining rules that are shown below:

$$\varepsilon_{ij} = \sqrt{\varepsilon_{ii}\varepsilon_{jj}} \text{ and } \sigma_{ij} = \frac{\sigma_{ii} + \sigma_{jj}}{2}. \quad (3.2)$$

3.2.3 Solid of Gold

The solid of gold (Au) is selected as the crystal solid walls since the Au substrate has a very basic crystal structure in the real situation, which makes it a suitable candidate to be used for studies related to the characteristic of surface structures. The potential function for solid walls that will be used are Morse potential. The equation is as shown:

$$U(r_{ij}) = D \left[e^{-2\alpha(r_{ij}-r_0)} - 2e^{-\alpha(r_{ij}-r_0)} \right], \quad (3.3)$$

where $D = 7.6148 \times 10^{-20}$ J, $r_0 = 3.0242 \text{ \AA}$ and $\alpha = 1.5830 \text{ \AA}^{-1}$. The equation and the value of D , r_0 and α were chosen from previous research. (Lincoln, Koliwad, & Ghate, 1967) The Au atom considered as electrically insulating material where the heat conduction through free electron is neglected.

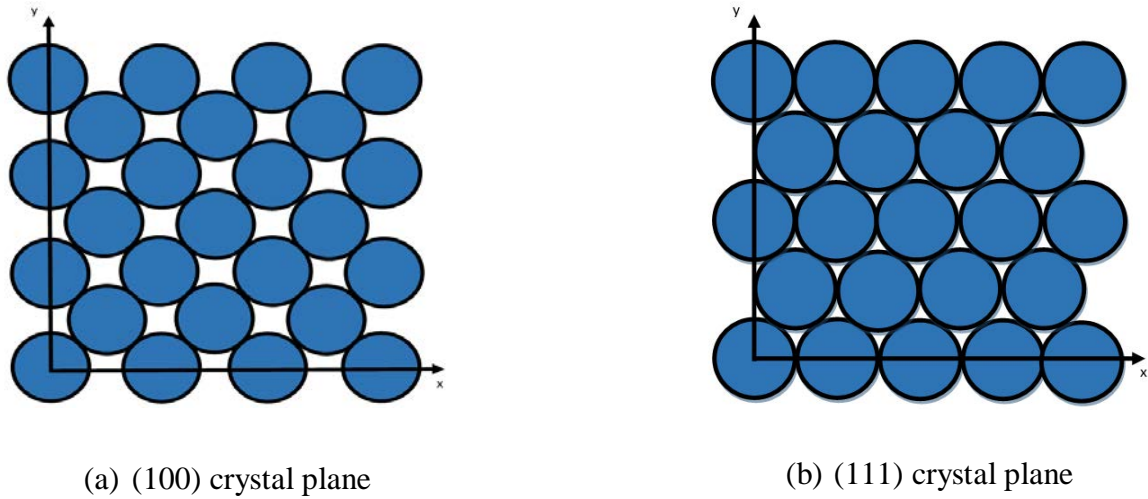


Figure 3.3: Surface structure of (100) and (111) crystal plane.

3.3 Boundary Condition

Depending on the computational resources or target system, the size of the MD simulation system varies from system to system. In general, the size of MD simulation systems is limited to a few hundred nanometers at the largest, with periodic boundary conditions (PBC) overcoming this limitation. Due to the above statement, the PBC will be applied in x - and y -directions. There was no PBC applied in z -direction since the temperature difference shall be applied to the system. The cut-off radius is truncated beyond the radius of 12 \AA all the way through the simulation for LJ and Morse potentials. The size of simulation system are set to be approximately $40.73 \times 40.73 \times 117.02 \text{ \AA}$ for (100) crystal plane and $40.32 \times 39.91 \times 118.22 \text{ \AA}$ for (111) crystal plane. Table 3.1 shows the number of solid atom in x -, y - and z -axes and in one layer based on the types of crystal plane and the number of liquid molecules for CH_4 liquid.

The number of solid atoms in x -, y - and z - axes are set separately to ensure that the simulation system size is about the same. The left and right side of the solid walls have the same number of solid atoms. The size of the simulation box is selected in such a way that the liquid molecules and solid atoms do not interact with the same molecule twice and do not interact with their own images from the simulation box. For CH_4 liquid, the distances in z -direction between the two parallel solid walls where the liquid film is filled, which is the liquid film thickness, is set to be 60 \AA . The thickness of the liquid film is set to ensure that the liquid molecules in the center of the simulation system are free from the influence of the solid walls interaction. In this study, the liquid alkane is set at the saturated liquid state at

$0.7 T_c$, where T_c is the critical temperature of the liquid. The critical temperature and liquid saturated density of $0.7 T_c$ are based on the previous study (Taku Ohara et al., 2011) where the critical liquid are 134.3K and the density of saturated liquid at $0.7 T_c$ are 378.6 kgm^{-3} .

Table 3.1: The size of the simulation system (Abdul Rafeq bin Saleman et al., 2017b)

Liquid Alkane	Type of crystal plane	Number of solid atom (x-, y- and z-axis)	Number of solid atom in one layer	Number of liquid molecules
CH ₄	(100)	$10 \times 20 \times 6$	200	1200
	(111)	$14 \times 16 \times 6$	224	1184

3.4 Simulation Detail

The simulation are pretty much the same as the real experiments. Firstly, prepare a sample which is a model system are selected consist of N particles and solve Newton's equations of motion for the system until the properties of the system are equilibrium where the system no longer change with time. After equilibration, the actual measurement is perform. Most errors during a computer experiment are similar to a real experiment, such as the measurement is too short or the sample is not properly prepared. To measure an observable quantity in a MD simulation, a function of the positions and momenta of the particles in the system has to be express (Daan Frenkel; Berend Smit, 1996).

The system is first raised to the target temperature of 133 K for the simulation setup of the non-shear system. After that, it is equilibrate until a uniform flow at target temperature are acquired. Then the different temperature setup is applied where both sides of the solid wall are set at low temperature while the high temperature is set at the center of the liquid alkane. Next step is the data acquisition for the temperature and heat flux.

For the shear system, the same first step is done which is to raise to the target temperature. After the uniform flow are acquired, the system are given a constant speed of 100 m/s on the left and right side of solid wall in the opposite direction. Then, a temperature control is set on the both sides of the solid walls. Next step are the data acquisition for the temperature and heat flux for about 10million time steps.

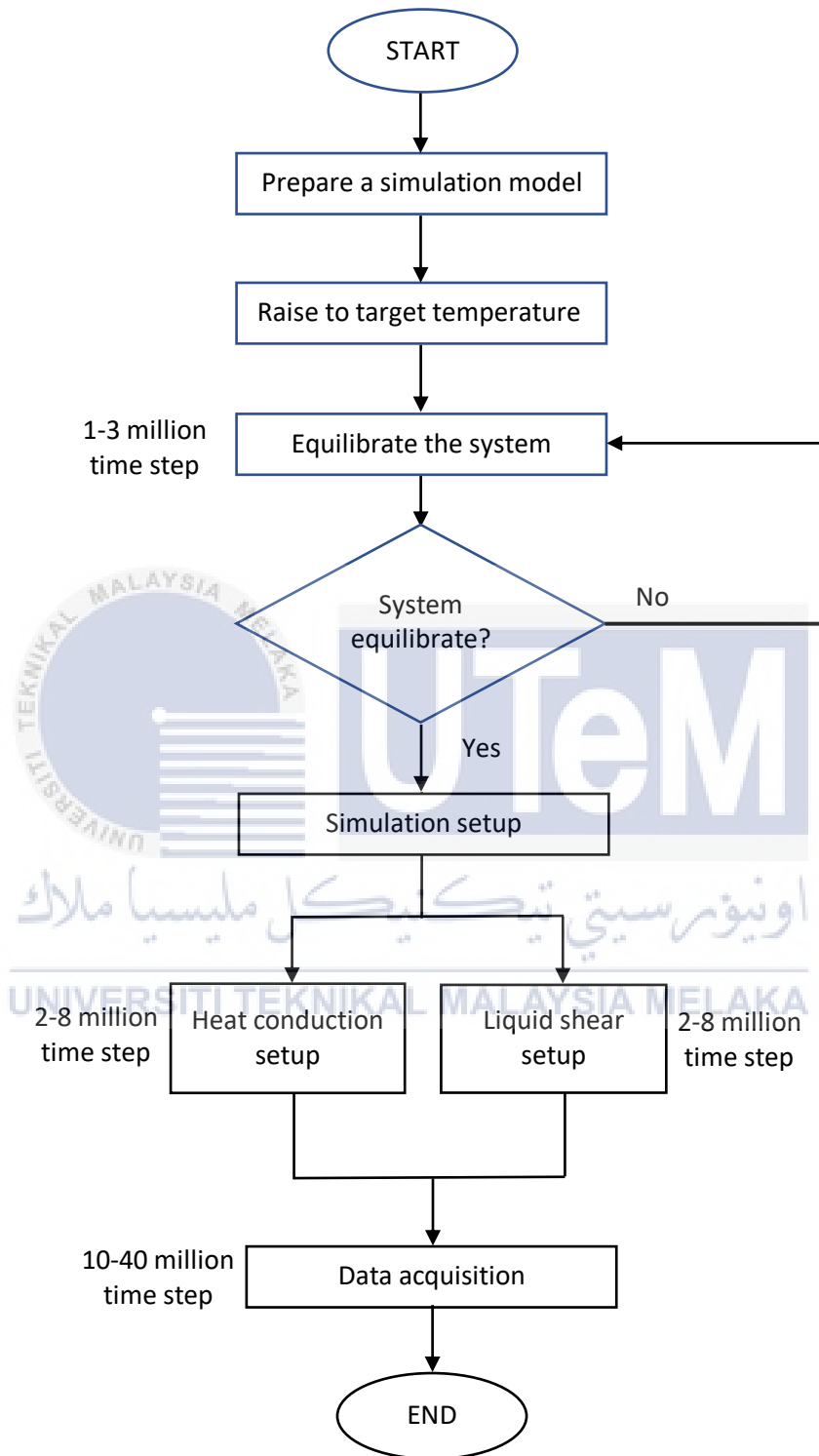


Figure 3.4: Flowchart of the simulation system.

3.4.1 Numerical Integration Method

Before starting the simulation, we have to choose the suitable time integration system. MD simulation is a tool that has been widely used to compute the motion of particles in a system. Consider a set of N particles with position of r and momentum of p . In many cases, algorithms of molecular dynamics are time reversible, meaning that the same sequence of steps returns to the starting point can be used by running the trajectory forward and backwards with the same number of steps. In the complex MD simulation system, the particles in the system are interconnected between one another. Due to that, it is impossible to come up with an analytical solution from the equation of motion. As such, the motion of particles or molecules in a system is predicted by a numerical integration method. In this research, a reversible references system propagator algorithm (r-RESPA) with multiple time step will be chose as the numerical integration method (Berne, 1999). The intermolecular motion and intramolecular motion uses 1 fs and 0.2 fs integration time steps, respectively.

3.4.2 Barostat and Thermostat

In this study, the temperature of the system is controlled by using velocity-scaling method throughout the simulation. For the pressure of the system, it was determined based on the density of the saturated liquid state that is controlled by the temperature of the system. Initially, the temperature system is slowly raise to the target temperature for 1 to 2 million time steps. The simulation system are maintained at constant temperature hereafter. The constant temperature of $0.7T_c$ of liquid alkane setup is run for 3 to 5 million time steps until a uniform temperature is acquired where T_c is the critical temperature. Once an equilibrium has been reached, liquid density is measured and the temperature controlled is removed from the simulation system. The density is measured before the controlled temperature is removed from the simulation system in order to ensure that the density of the liquid is at the saturate liquid state. Next, the simulation system are applied with heat flux and shear given to the liquid.

For the heat flux, both side of the solid walls are set as low temperature while at the center of the liquid is set as high temperature that are shown in Figure 3.1 which will generate the constant heat flux across the simulation system. A temperature control in a partial region is set up on both sides of the solid walls. The control region begins on both sides of the solid walls from the second outermost surface layer and ends at 4 \AA towards the center of the system in z-direction. For the liquid shear, a shear is given to the system by sliding the two

solid parallel walls at a constant speed and in the opposite direction as shown in figure 3.2. The outermost layer of solid atoms in the x-direction is set at a constant speed. A Couette-like macroscopic flow is generated in the sheared liquid and the flow energy is converted into thermal energy by viscous heating. The viscous heating generates heat and the heat is transferred via heat conduction to the parallel solid walls. The variation in the time steps depends on the molecular length of liquids, where longer liquid molecules require more time steps to have the obtained data converged.

3.4.3 Measurement of Structural Quantities

3.4.3.1 Density distribution

The density distribution in a simulation system provides an insight into the liquid condition. To calculate density distribution, it can be calculated by dividing the simulation system into several slabs, each of which has a thickness of about 0.02 Å in the z-direction. The average number of molecules or pseudoatoms in the slab is counted when calculating density in each slab. By dividing the average number of molecules in the unit of volume (m^3) into the slab size, the value of the local number density (m^{-3}) is given. The number density (m^{-3}) is then multiplied by the molar mass of liquid (16.043 gmol^{-1}) and divided by the Avogadro number ($6.022140857 \times 10^{23}$) which will give the density (kgm^{-3}) for the slabs. For CH_4 liquid, the density of each slab is measured based on number of molecules. On the density distribution, the behaviour of the absorption layer of liquid molecules and the surface layer of solid atom will be discussed later where the absorption layer of liquid molecules represent the density distributions of the liquid oscillate near the solid walls and the peak, and the surface layer is the layer of solid atoms that are closest to the liquid film.

3.4.4 Measurement of Physical Quantity

3.4.4.2 Temperature

Once the temperature on both solid of the solid wall and the liquid has been setup, a temperature distribution and velocity distribution will produced in the liquid alkane confined with solid walls. For the temperature, the system can be divided into a number of slabs in order to calculate the local temperature in the simulation system. Different slab thickness

will be used in the temperature distribution due to the thickness of the absorption layers for the liquid is different between each layer and types of crystal (Abdul Rafeq bin Saleman et al., 2017a). The dividing line between each slab are to be used to measure the average heat flux throughout the system as a control surface. The temperature of each slab shall be calculated from the kinetic energy of the random velocity of molecules. For the shear system, the random component of the velocity will be calculated by subtracting the local macroscopic flow velocity of the system from the overall velocity of the pseudoatoms.

3.4.5 Measurement of Slip Length

As stated in Chapter 2, the slip length is defined as the linearly extrapolated velocity of liquid from the S-L interface into the solid walls, where the tangential velocity of liquid coincides with the velocity of solid walls. The surface structure of the solid walls influences the slip near the S-L interface. Therefore the slip length will be measured with the presences of velocity distribution of the shear system and will be compared between two crystal planes. In the previous study, the slip length was seen to be directly proportional with the momentum boundary resistance. Thus, the slip length is measured to study the characteristic of the momentum transfer over the S-L interface.

3.4.5 Measurement of Heat Flux

As described in Chapter 2, the heat flux can be obtained by modifying the expression under the assumption of uniformity of the system and no macroscopic fluid flow. In this study, the heat flux data will be collected from many body potentials and the MD expression of heat flux extended for many body potential are to be used. The heat flux, J_z across control surface S_{xy} is given as follows (Taku Ohara, 1999a; Abdul Rafeq bin Saleman et al., 2017a; Torii & Ohara, 2007):

$$J_z S_{xy} = \sum_i \left[\left(\frac{1}{2} m v_i^2 + U \right) / 1 \right] \frac{v_{i,z}}{|v_{i,z}|} + \frac{1}{2} \sum_i \times \sum_{j>i} [F_{ij} (v_i + v_j)] \frac{z_{ij}}{|z_{ij}|} \quad (3.4)$$

where v_i is the velocity vector of particle i and $v_{i,z}$ is the z -component of the velocity vector. F_{ij} is the intermolecular force acting on particle i due to the pair potential defined between i and j . z_{ij} is the distance along the z -axis of particle i and j . \sum_i is the summation of all particles in the system or slab and $\sum_i \sum_{j>i}$ is the summation of all pairs of particles which interact across the control surface.

As described in Chapter 2, the heat flux consist of two terms. The first term represents the kinetic and potential energy of molecules and the second term represents the transfer of intermolecular energy due to intermolecular forces between molecules. In addition, the heat flux equation is further divided into three degrees of freedom (DOF) according to the particle motion. The energy transfer between the particles takes place during the particle motion process. With regards to the translation motion of particle i , the rate of kinetic energy increase of molecule i , is equal to the power due to the force acting on molecule i at molecule i velocity (Taku Ohara, 1999b). As a result, the force acting on the molecule i and the velocity of the molecule i can be decomposed into x -, y - and z -axis by molecular movement. As such, the second term of Eq. (4) from the force of the intermolecular interaction between liquid and solid can be further decomposed into the x -, y - and z -DOFs in such manner that:

$$\mathbf{F}_{ij} \cdot \mathbf{v}_i = F_{ij,x} \cdot v_{i,x} + F_{ij,y} \cdot v_{i,y} + F_{ij,z} \cdot v_{i,z} \quad (3.5)$$

where $F_{ij,x}$ is the x -component of intermolecular force acting between particles i and j . $v_{i,x}$ is the velocity in the x -component of particle i . Each of the x -, y - and z -terms on the right side of Eq. (5) represents the intermolecular energy transfer due to the particle motion in each DOF.

3.4.6 Thermal Boundary Resistance

The thermal boundary resistance (TBR) is determined by the calculation of the ratio of the Temperature Jump (TJ) to the heat flux, as follows:

$$\text{TBR} = \frac{\Delta T}{J} \quad (3.7)$$

where ΔT represents temperature jump at the interface between the solid wall and the liquid which was obtained by the procedure, while J represent the heat flux across the interface. Eq. (3.7) calculation for the TBR will be used due to most of them used the same equation to calculate TBR in the previous study.

CHAPTER 4

RESULT AND DISCUSSION

4.1 Introduction

This chapter examines the thermal energy transfer and momentum transfer at solid-liquid (S-L) interfaces of liquid alkanes in contact with (100) and (111) crystal plane of face-centered cubic (FCC) gold. A constant heat flux is applied across the simulation system by controlling the temperature of the solid walls at a different temperature. The analysis between shear system and non-shear system is observed and has been discussed in terms of density, temperature, slip length and thermal boundary resistance on the S-L interfaces.

4.2 Density

The density distribution has been obtained by dividing the simulation system into rectangular slabs. The thickness of this rectangular slabs is relatively 0.02 \AA in the z -direction. Figure 1 and 2 illustrates the density distribution for (100) and (111) crystal plane, while Figure 3 represents the liquid methane for (100) and (111) crystal plane. In the past studies, the density distribution of liquid oscillates near the S-L interfaces. The oscillation disappears apart from the S-L interface and the flat distribution appears at the center of the simulation system. The peaks of the oscillation are here referred to as the absorption layers, and the flat distribution is here referred to as the bulk-like region.

4.2.1 Solid walls of (100) and (111) crystal plane

In the system, the outermost layer of solid atoms was set to be fixed on its lattice position and the atoms for the layer which is closer to the outermost layer of solid atoms are hardly fluctuate compared to the layers of solid atoms that are further away from the outermost layer. Due to the fluctuations of the solid atoms increases as the position of the layer of solid atoms approaches to the interface, the peak height of the density for the layers of solid atoms is decline as the layer is closer to the S-L interface. The surface layer of solid atoms is the layer of solid atoms closest to the S-L interface.

Figure 1 and Figure 2 illustrates the density distribution for CH₄ liquid contacting surfaces of (100) and (111) crystal plane where the red line represent CH₄ liquid and the green line at the left and right side represent the solid wall for (100) and (111) crystal plane. It can be observed that the surface layer of solid atoms has different peak heights for the two different types of crystal plane. By referring to Figure 4.1 and Figure 4.2, the surface layer of solid atoms of (100) crystal plane has the lower peak height in terms of density than the surface layer of solid atom of (111) crystal plane although the setting was almost identical for both crystal planes, such as the target temperature which is controlled to be about 0.7T_c at a steady state.

However, there are certain setting specifically for its own crystal plane such as the size of the simulation cell, the number of solid atoms in x, y and z-axis and the number of molecules for CH₄ liquid which has been shown in Chapter 3. From there, we can know that different types of crystal plane will generate different density distribution.

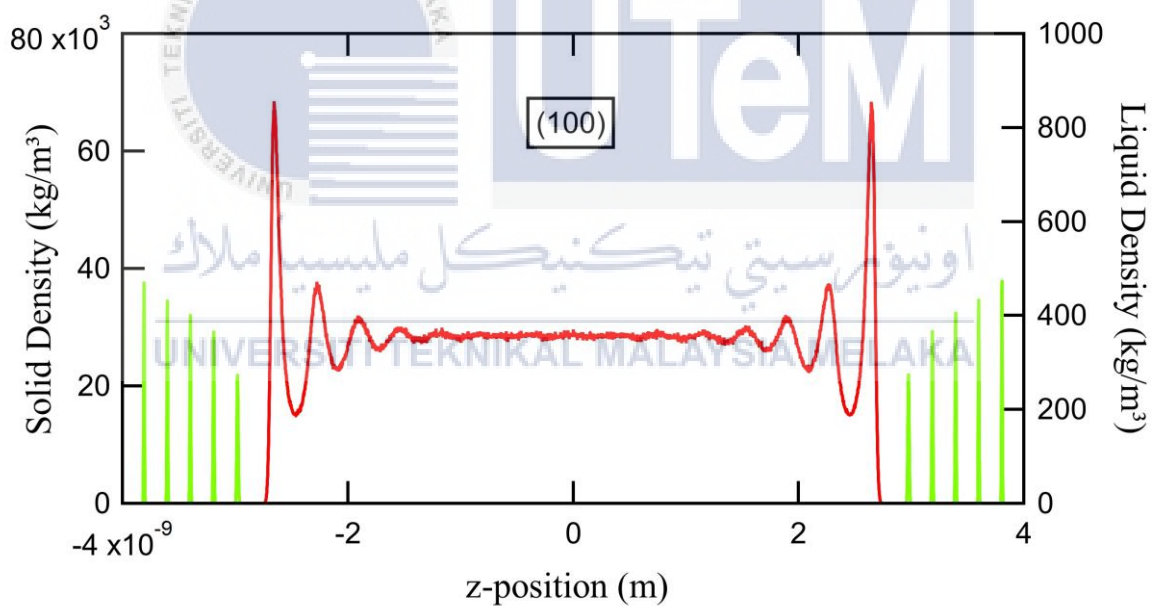


Figure 4.1: Density distribution of (100) crystal plane.

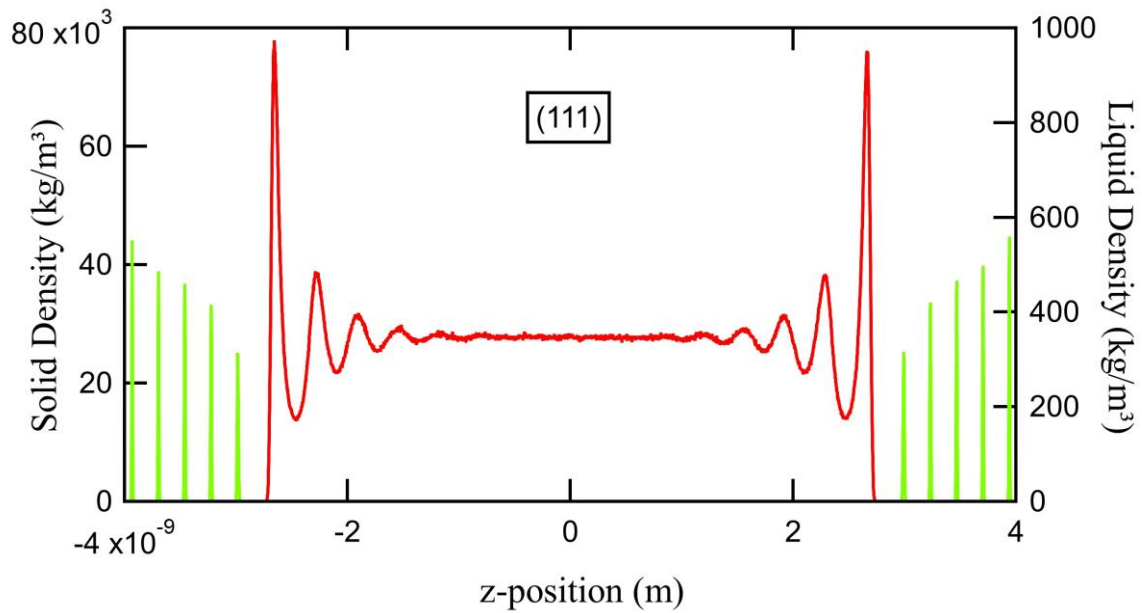


Figure 4.2: Density distribution of (111) crystal plane.

4.2.2 Liquid methane of (100) and (111) crystal plane

In the past studies, it is known that the absorption layers of liquid molecules onto the solid surface is represented by the density distribution of the liquid oscillate near the solid walls. By referring to Figure 4.3, the adsorption layer of liquid molecules that contacts the solid wall surface is referred as the first adsorption layer. The first adsorption layers of liquid among the FCC crystal planes show different packing density values even though all of the systems were set to be at the same temperature. Therefore, the correlation between the peak height of the density of the surface layer of solid atoms and the packing densities of the first adsorption layer of liquid has occurred.

As seen in Figure 4.3, the packing density of the first absorption layer of the liquid molecules for (100) crystal plane is can be seen to be lower than the first absorption layer of the liquid methane for (111) crystal plane. It can be clarify that the packing density of the liquid molecules in the first adsorption layer is influenced by the density of solid atoms in the surface layer where the surface layer of solid atom is the layer of solid atoms that are closest to the liquid film. Hence, higher peak height of the surface layer of solid atoms appears to generate higher packing density of the first absorption layer of liquid molecules. As observed in Figure 4.3, the packing density of the first absorption layer decreases with the increase in number of molecule of the liquids. Figure 4.4 shows the density distribution for (100) and (111) crystal planes in the simulation, making it easier to observe and analyse the density distribution.

For the shear cases, the density distribution for both solid walls and CH₄ liquid is found to be the same as non-shear cases, although the system on the left and right side was set to 100ms⁻¹ in the opposite direction, respectively. Thus it can be clarified that the shear in the simulation system does not affect the density. This was also verified in the previous study (Abdul Rafeq bin Saleman et al., 2017a).

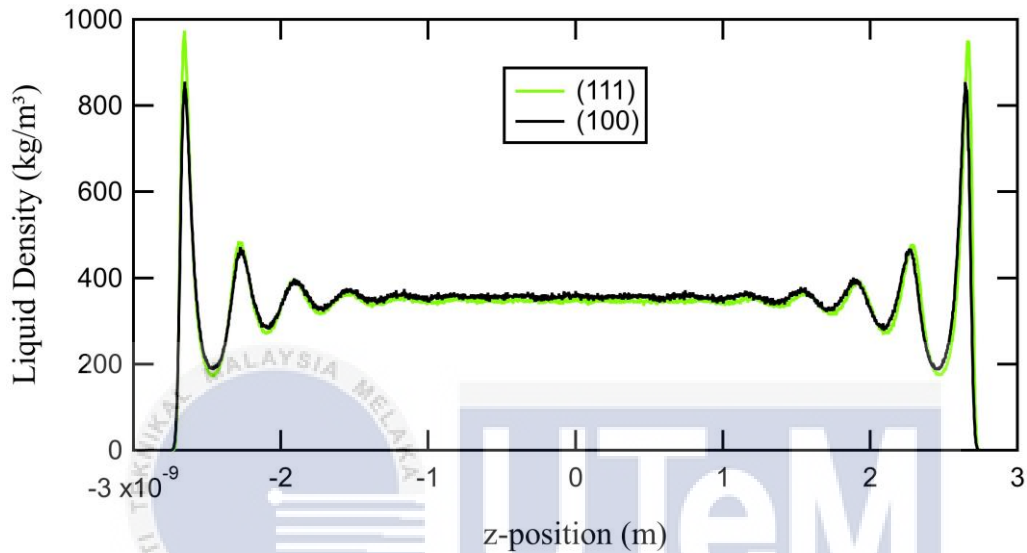


Figure 4.3: Density distribution of liquid methane of (100) and (111) crystal plane.

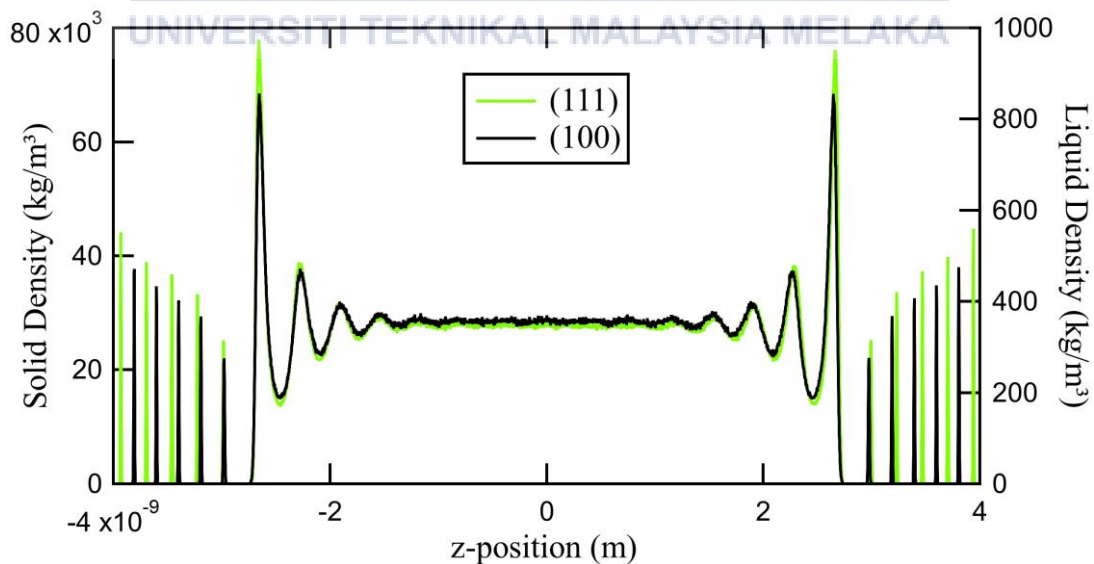


Figure 4.4: Density distribution for (100) and (111) crystal plane.

4.3 Temperature

4.3.1 Non-shear system

In the present system, the constant heat flux was applied across the simulation system by controlling the temperature on the left and right sides of the solid walls. The method used to control the temperature is by using velocity-scaling method. The controlling temperature setup was run for 1 to 5 million time steps until a steady state is acquired. The liquid methane in the system cannot reach the gas state because it will be out of the simulation cell size if it has reached the gas state. Therefore, CH₄ liquid was set within the range of the critical temperature, T_c that have been known the critical temperature for CH₄ liquid is 190K and the triple point temperature.

The average temperature of the CH₄ liquid was set at 0.7T_c in order to prevent it from becoming gas state. The value of 0.7T_c is equal to 133K. The simulation system was divided into several slabs in order to calculate the system's temperature distributions. A different slab definition was used to measure the local temperature and local velocity of the system since the thickness of the adsorption layers for liquid varies between layers. A typical slab definition of the temperature profile for CH₄ liquid contact with (100) crystal plane is shown in Figure 4.5. Although only (100) crystal plane was presented, the same method was used on (111) crystal plane.

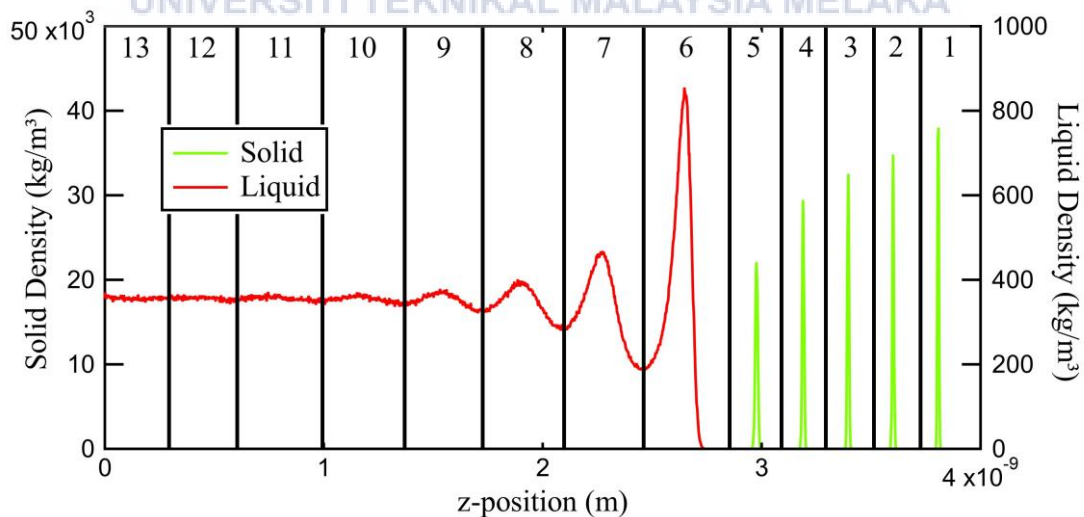


Figure 4.5: Definition of slab for the temperature and velocity distribution for (100) crystal plane.

Each layer of solid and liquid molecules was assigned a slab. Only the right side of the system is shown here, since the slab definition of the system for both sides is symmetrical. Therefore, the number of slabs on the left side of the simulation system is the same as on the right side. As seen in Figure 4.5, there are 13 slab on the right side of the simulation system which makes it 26 slab for the both side. To measure the average heat flux across the system, the dividing line between each slab was used as a control surface. For each pseudoatom located in the slab, the temperature of the system was calculated from the kinetic energy corresponding to the random component of velocity.

Figure 4.6 and Figure 4.7 shows the temperature distribution of the non-shear system for (100) and (111) crystal plane while Figure 4.8 illustrates the temperature distribution for the both crystal plane types. The dash line in the figure represents the S-L interfaces. Based on Figure 4.6 and Figure 4.7, it can be observed that there are temperature jump (TJ) at the left and right side of the S-L interfaces. The TJ is defined as discontinuity of temperature at the S-L interfaces. The TJ at the S-L interfaces is measured to further understand the characteristics of thermal energy transfer across the S-L interfaces that will be used to examine thermal boundary resistance (TBR) for both types crystal plane.

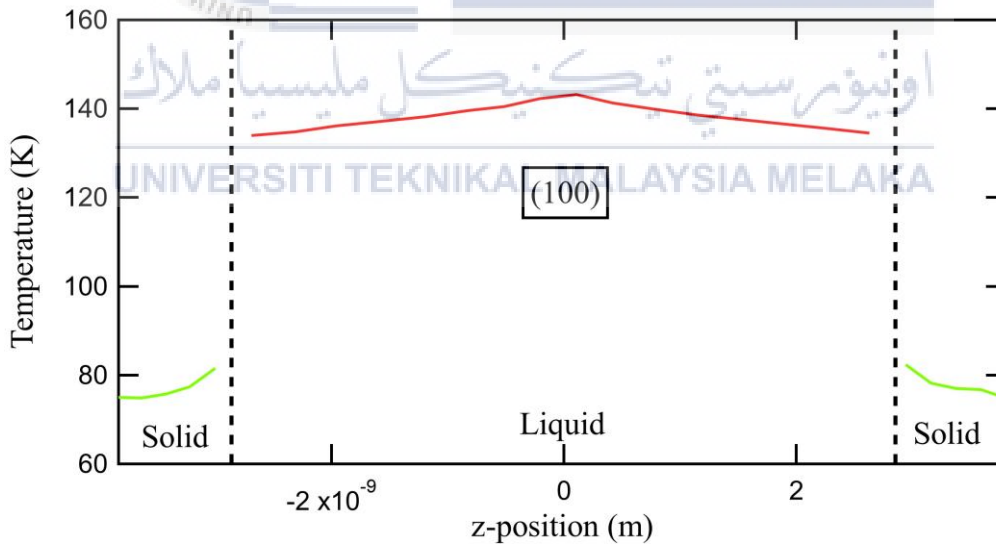


Figure 4.6: Temperature distribution of non-shear case for (100) crystal plane. The dash line represents the S-L interfaces.

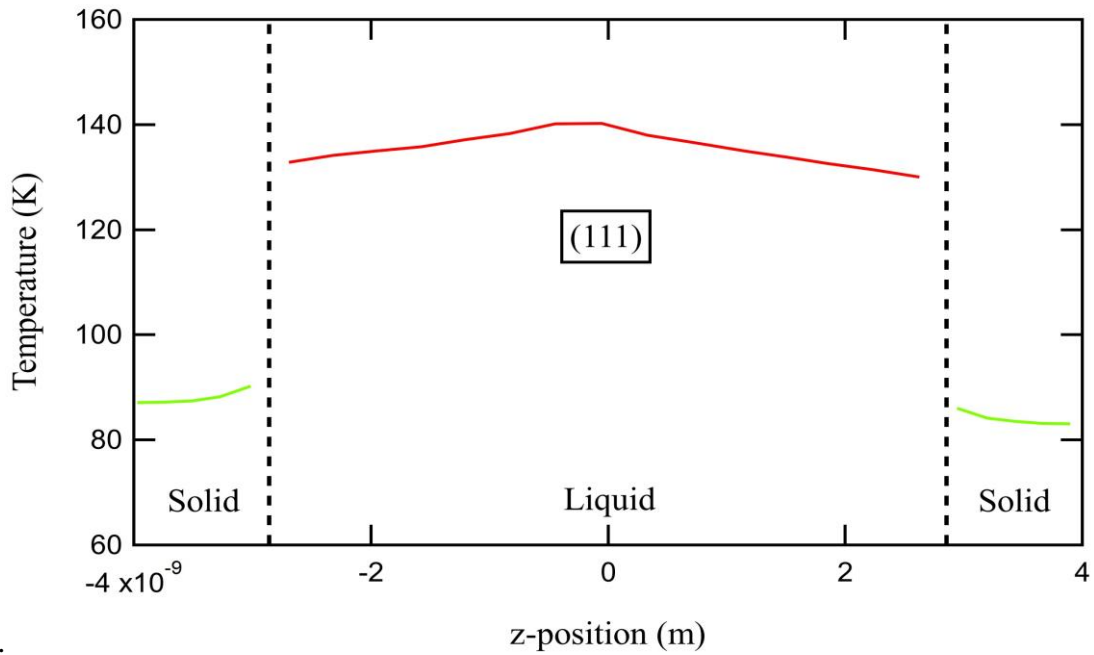


Figure 4.7: Temperature distribution of non-shear case for (111) crystal plane.

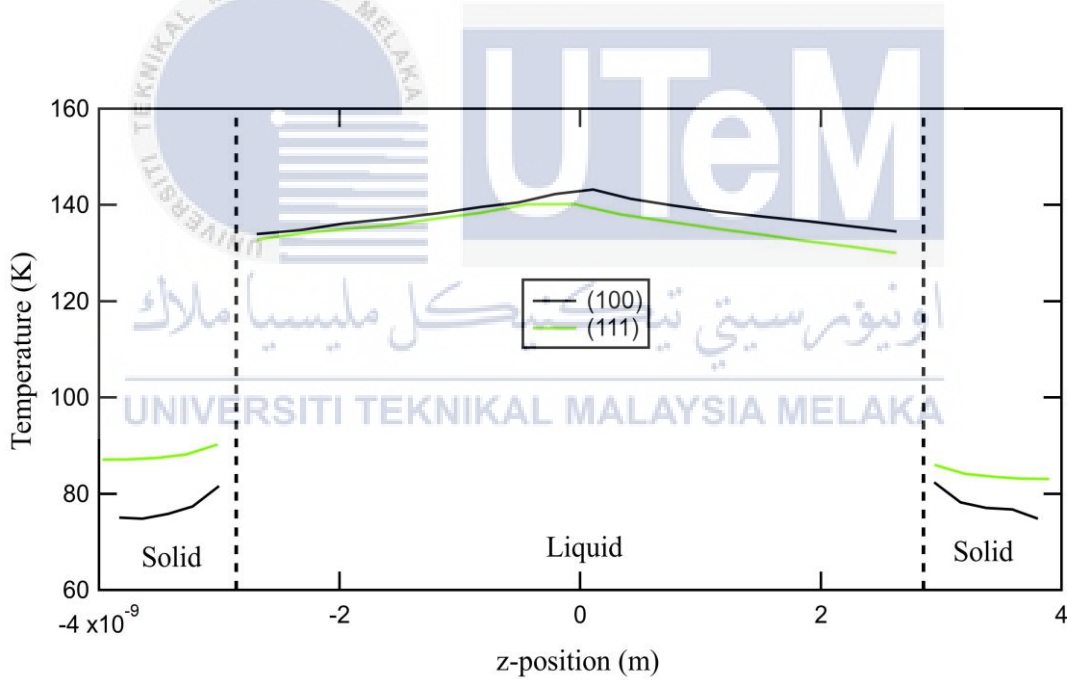


Figure 4.8: Temperature distribution of non-shear system for (100) and (111) crystal plane.

The appearance of TJ at the solid–liquid interfaces was also reported in the previous study where the cause of the appearance of temperature jump was explained to be a phonon mismatch at the interface (Barisik & Beskok, 2014; Torii et al., 2010). Phonon mismatch occur when phonons are transported across a material interface, they experience conversion

of reflection, transmission and mode, resulting in a local temperature jump at the interface (Li & Yang, 2012).

In order to calculate the TJ, the temperature distributions of solid walls were linear and the temperature distributions of liquid alkanes were quadratic and both lines were then extrapolated to the midpoint of the equilibrium positions of the surface layer of solid atom and the first adsorption layer of liquid molecules, where the temperature difference between the solid and the liquid alkane was determined. The evaluation of the TJ can be seen in Figure 4.9 where it exhibit the left side of the temperature distributions of (100) crystal plane. The circle at the dashed line indicates the extrapolation value for the TJ at the S-L interface. The TJ for (111) crystal plane were also measured in the study although only (100) is shown. It is observed that (100) crystal plane has a higher TJ compared to the (111) crystal plane. The value of the TJ will be shown later in the next subchapter where the TJ value is used to study the thermal boundary resistance in the simulation system.

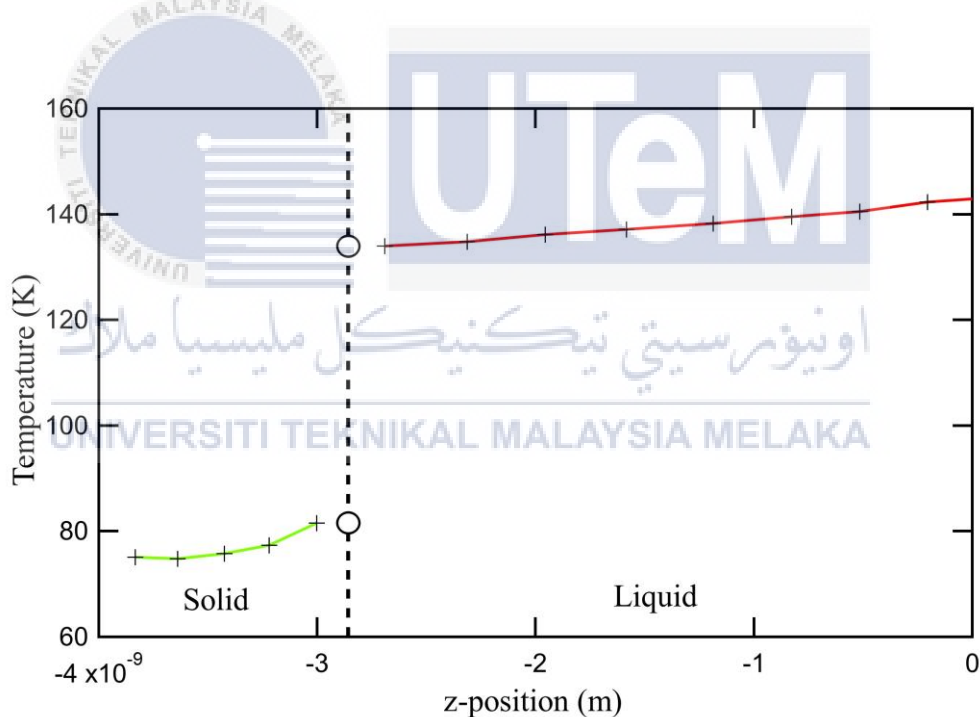


Figure 4.9: The temperature distribution of non-shear system for the left side of (100) crystal plane. The dash line represents the S-L interface.

4.2 Shear system

For the shear setup of the simulation system, the liquid film was sheared by moving the right and left side of the solid wall at a constant speed of 100ms^{-1} in the opposite direction that has been shown in Figure 3.2. The local macroscopic flow velocity of the

system was subtracted from the overall velocity of the pseudoatoms. In order to calculate the velocity of the system. The velocity jump (VJ) referred to as velocity discontinuity and TJ will be discussed here. The same method is used to measure the TJ that has been explained in the non-shear system. Same method is used to measure VJ, but the difference is that the velocity distribution of liquid alkanes was linear. Figure 4.10 illustrates the velocity distribution of the shear system that was given a constant speed of 100ms^{-1} for (100) and (111) crystal plane. By referring to the S-L interface based on Figure 4.10, the velocity jump takes place on both sides of the simulation system and each crystal plane has different VJ. From what it was seen, for (111) crystal planes case, it has larger VJ compared to (100) crystal plane. It is known that (111) crystal plane has a smoother surfaces than (100) crystal plane. Therefore, it is discerned that different surface structure will produce different VJ, where this statement have been affirmed in the past study (Abdul Rafeq bin Saleman et al., 2017a).

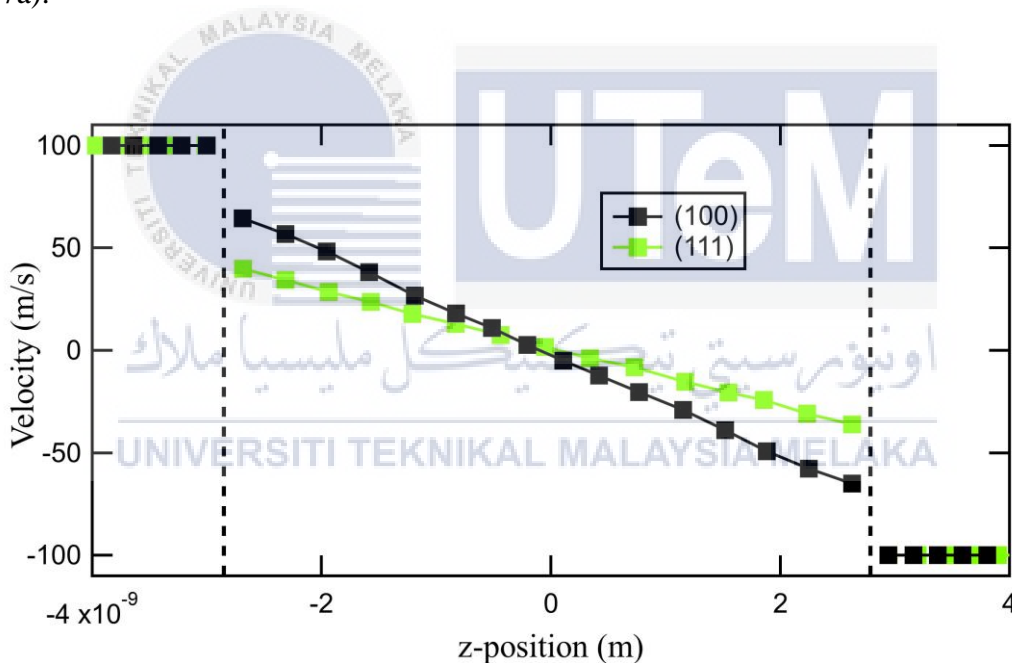


Figure 4.10: Velocity distribution of shear system for (100) and (111) crystal plane. The square marker represents the number of slab for the simulation system. The dash line on the left and right side of the simulation system represents S-L interfaces.

Figure 4.11 and Figure 4.12 shows the temperature distributions of (100) and (111) crystal plane for the shear system. It can be seen that for liquid contacting (100) crystal plane, the TJ is higher as compared to (111) crystal plane. The heat conduction from the liquid to the solid over the S-L interface occurred due to viscous heating caused by the shear given to

the liquid. For the case of (100) crystal plane, which produced a lower VJ than (111) crystal plane, high shear rate and large viscous heating in the liquids will result. This large viscous heating will then produce a large amount of heat at the center of the liquid that has to be transferred to the solid wall. As a result, a more parabolic shape of temperature distribution was discovered. Furthermore, large amounts of heat transferred through the S-L interface produces large TJ. For that reason, it can be determined that a higher surface roughness increases the TJ across the S-L interfaces. For the comparison of the temperature distribution between shear and non-shear system, the TJ value from the non-shear system seems to be larger than the TJ from the shear system for the both types of crystal plane. Based on this finding, it is understood that different surface structure and shear added to the system will leads to different characteristic of thermal energy transfer.

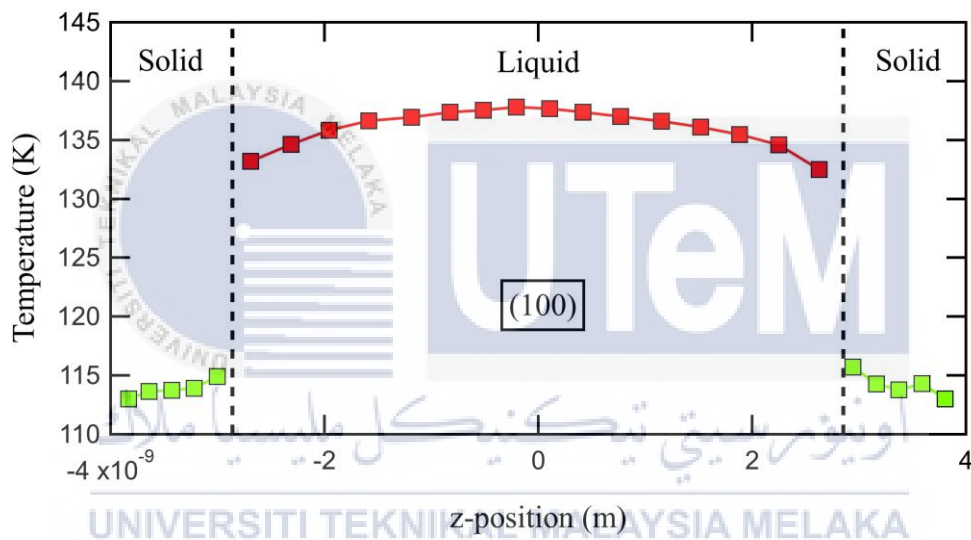


Figure 4.11: Temperature distribution of shear for (100) crystal plane.

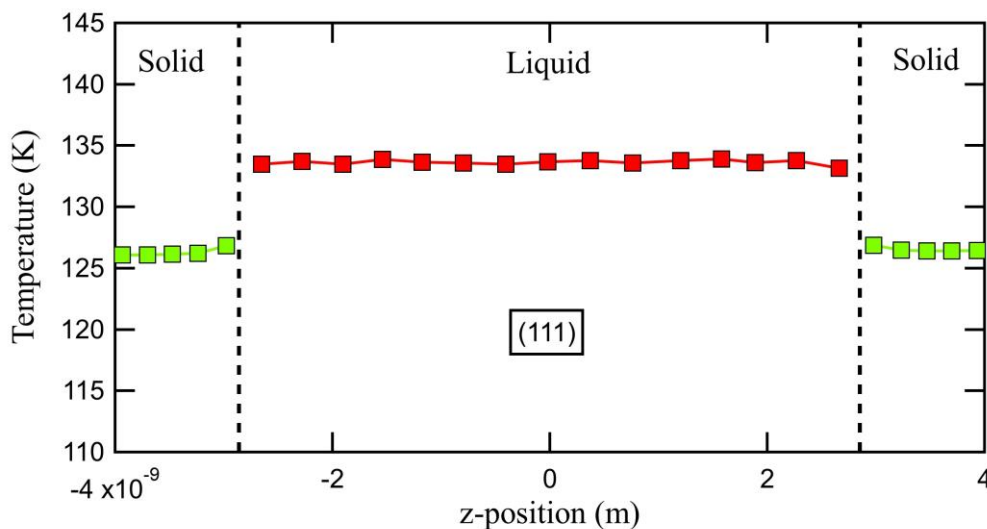


Figure 4.12: Temperature distribution of shear for (111) crystal plane.

4.3 Slip Length

As outlined in Chapter 3, the slip length is defined as the linear extrapolate velocity of the liquid from the S-L interface into the solid walls, where liquid tangential velocity disappears or is equal to zero. The slip length is measured only for the shear system where the non-shear has no shear involving the simulation process. Figure 4.13 shows the slip length of (111) crystal plane, where the slip length was measured until it reached the right side of the solid walls. The same method are used to measure the slip length of (100) crystal plane. Table 4.1 shows the slip length for (100) and (111) crystal plane.

Higher surface roughness has previously been reported to decrease the slip length (Abdul Rafeq bin Saleman et al., 2017a). This can be proved when it is found that the slip length differs significantly between crystal planes where the slip length for (111) crystal plane is larger than the slip length of (100) crystal plane as displayed in Table 4.1. As stated in Chapter 4.2, the surface of the (111) crystal plane is smoother than the (100) crystal plane. The surface structure of the solid walls produced this difference between this two types of crystal planes. It is therefore noted that the length of the slip is correlated with the surface structure of the solid walls.

In Chapter 3, it was suggested that the results for the slip length could be analysed and measured to study the momentum transfer characteristic of the S-L interface where the slip length was found to have a similar trend with momentum boundary resistance. Thus it can also be stated that shorter slip length will results in a greater momentum transfer.

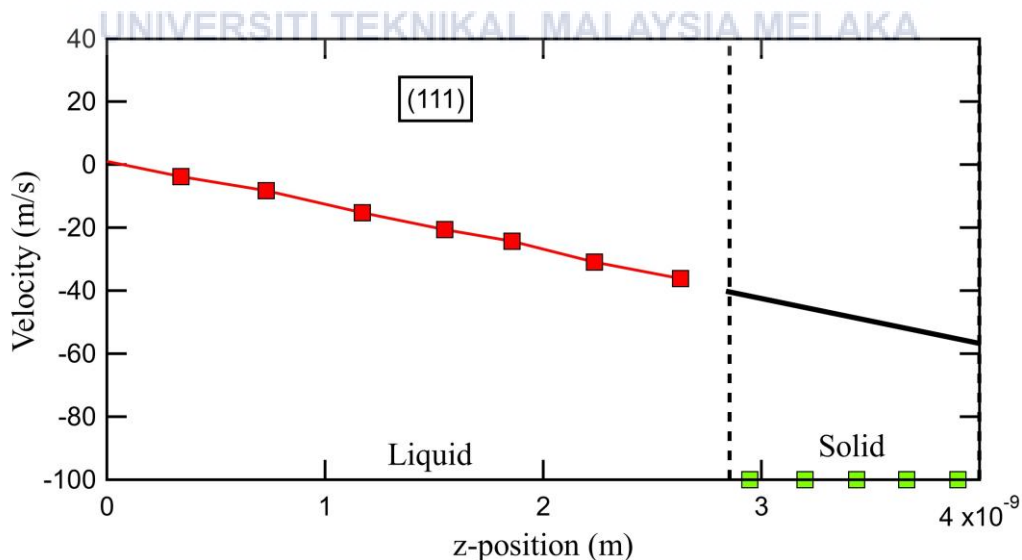


Figure 4.13: The slip length of the right side of (111) crystal plane. The black lines indicates the slip length and the dashed line represents S-L interface.

Table 4.1: The slip length of the shear system for (100) and (111) crystal plane.

Crystal Plane	Slip length (m × 10 ⁻⁹)
(100)	1.4892
(111)	4.5319

4.4 Heat Flux and Thermal Boundary Resistance

The thermal boundary resistance (TBR) was determined to understand the characteristic of thermal energy transfer at the S-L interface by using Eq. 3.7 as follows:

$$\text{TBR} = \frac{\Delta T}{J} \quad (3.7)$$

where ΔT is the TJ at the S-L interface from the temperature distribution and J is the heat flux throughout the simulation system. The TJ for CH₄ liquid in contact with (100) and (111) crystal plane was calculated and tabulated in Table 4.2 and 4.3 together with the heat flux and TBR data for the both setup. Although the system was set at approximately the same reduced temperature and similar condition, there are differences in TJ and heat flux values between the two crystal plane cases and the system setup. The TBR value for (100) crystal plane was found to be larger than (111) crystal plane for non-shear setup while the TBR for (111) is larger than (100) crystal plane for shear setup. For non-shear cases, this can be proven when the TBR is correlated with the peak height of the surface layer of solid atoms. Thus, it can be assumed that the large number of atoms presents at the surface layer of solid atoms will generate high thermal energy transfer and low TBR at the S-L interfaces. For the shear cases, due to the large TBR, it is ineffective for the thermal energy transfer. Based on Table 4.2 and 4.3, it is concluded that the surface structure of crystal plane and the shear system affects the characteristic thermal energy transfer at the S-L interfaces.

Table 4.2: The overall results for TBR of non-shear system.

Crystal Plane	Temperature Jump (K)	Heat Flux (MW/m ²)	TBR (m ² K/W × 10 ⁶)
(100)	52.4	395.5	0.1325
(111)	42.6	385.9	0.1104

Table 4.3: The overall results for TBR of shear system

Crystal Plane	Temperature Jump (K)	Heat Flux (MW/m ²)	TBR (m ² K/W × 10 ⁶)
(100)	18.3	113.8	0.1591
(111)	7.3	44.7	0.1633

CHAPTER 5

CONCLUSION AND RECOMMENDATION

5.1 Conclusion

In this study, the characteristic of thermal energy and momentum transfer consists of the two different types of face-centered cubic (FCC) crystal of gold with the surfaces of (100) and (111) contacting liquid alkanes at S-L interface were examined. For density, it is found that the absorption layer of liquid and the surface layer of solid atoms have been influenced by the types of crystal plane, whereas the crystal plane with a larger number of solid atoms will generate a higher density. Moreover, the packing density of the liquid molecules in the first adsorption layer is influenced by the density of solid atoms in the surface layer where the surface layer of solid atom is the layer of solid atoms that are closest to the liquid film. The density for shear and non-shear was found to be the same, therefore the shear applied in the simulation system does not affect the density.

For temperature and velocity, it can be determined that higher surface roughness will increase the temperature jump across the S-L interfaces while reducing its slip length. Therefore, it can be assumed that different surface structure and shear added to the system will lead to different characteristics of thermal energy transfer. For thermal boundary resistance, it was concluded that the surface structure of crystal plane and the shear system affects the characteristic of thermal energy transfer undoubtedly at the S-L interfaces where a low thermal resistance are important in determining an overall performances of the system.

5.2 Recommendation

After this study was done, there are few recommendation that will be issued. The first is that it is recommended that the future study include investigation of the molecular length of liquid alkanes when comparing the shear and non-shear system where it is essential to know the characteristic of other types of liquid alkanes for a better future application.

REFERENCES

- A., R. (1964). Correlations in the Motion of Atoms in Liquid Argon. *Physical Review*, 136, A405-- A411.
- Andersen, H. C. (1980). Molecular dynamics simulations at constant pressure and/or temperature. *The Journal of Chemical Physics*, 72(4), 2384–2393. <https://doi.org/10.1063/1.439486>
- Bair, S., McCabe, C., & Cummings, P. T. (2002). Calculation of viscous EHL traction for squalane using molecular simulation and rheometry. *Tribology Letters*, 13(4), 251–254. <https://doi.org/10.1023/A:1021011225316>
- Bair, S., McCabe, C., McCabe, C., Cummings, P. T., & Cummings, P. T. (2002). Comparison of nonequilibrium molecular dynamics with experimental measurements in the nonlinear shear-thinning regime. *Physical Review Letters*, 88(5), 583021–583024. <https://doi.org/10.1103/PhysRevLett.88.058302>
- Barisik, M., & Beskok, A. (2014). Temperature dependence of thermal resistance at the water/silicon interface. *International Journal of Thermal Sciences*, 77, 47–54. <https://doi.org/10.1016/j.ijthermalsci.2013.10.012>
- Berendsen, H. J. C., Postma, J. P. M., Van Gunsteren, W. F., Dinola, A., & Haak, J. R. (1984). Molecular dynamics with coupling to an external bath. *The Journal of Chemical Physics*, 81(8), 3684–3690. <https://doi.org/10.1063/1.448118>
- Berne, B. J. (1999). Molecular Dynamics in Systems with Multiple Time Scales: Reference System Propagator Algorithms. *Computational Molecular Dynamics: Challenges, Methods, Ideas: Proceedings of the 2nd International Symposium on Algorithms for Macromolecular Modelling, Berlin, May 21--24, 1997*, 297–317. https://doi.org/10.1007/978-3-642-58360-5_16
- Bhushan, B. (1973). Principles and Applications of Tribology. In *Tectonophysics* (Vol. 17). [https://doi.org/10.1016/0040-1951\(73\)90070-X](https://doi.org/10.1016/0040-1951(73)90070-X)

Daan Frenkel; Berend Smit. (1996). *Understanding Molecular Simulation*.
[https://doi.org/https://doi.org/10.1016/B978-0-12-267351-1.X5000-7](https://doi.org/10.1016/B978-0-12-267351-1.X5000-7)

Dubbeldam, D., Calero, S., Vlugt, T. J. H., Krishna, R., Maesen, T. L. M., & Smit, B. (2004). United atom force field for alkanes in nanoporous materials. *Journal of Physical Chemistry B*, 108(33), 12301–12313. <https://doi.org/10.1021/jp0376727>

Eggimann, B. L., Siepmann, J. I., & Fried, L. E. (2007). Application of the TraPPE force field to predicting isothermal pressure-volume curves at high pressures and high temperatures. *International Journal of Thermophysics*, 28(3), 796–804. <https://doi.org/10.1007/s10765-007-0208-9>

Evans, D. J. (1983). Computer “experiment” for nonlinear thermodynamics of Couette flow. *The Journal of Chemical Physics*, 78(6), 3297–3302. <https://doi.org/10.1063/1.445195>

Ewen, J. P., Heyes, D. M., & Dini, D. (2018). Advances in nonequilibrium molecular dynamics simulations of lubricants and additives. *Friction*, (Md). <https://doi.org/10.1007/s40544-018-0207-9>

Foiles, S. M., Baskes, M. I., & Daw, M. S. (1986). Embedded-atom-method functions for the fcc metals Cu, Ag, Au, Ni, Pd, Pt, and their alloys. *Physical Review B*, 33(12), 7983–7991. <https://doi.org/10.1103/PhysRevB.33.7983>

Girifalco, L. A., & Weizer, V. G. (1959). Application of the Morse Potential Function to Cubic Metals. *Physical Review*, 114(3), 686–687. <https://doi.org/10.1103/PhysRev.114.686>

Guevara-Carrion, G., Hasse, H., & Vrabec, J. (2012). Thermodynamic properties for applications in chemical industry via classical force fields. *Topics in Current Chemistry*, 307, 201–250. https://doi.org/10.1007/128-2011_164

HOOVER, W. G. (1985). Canonical Dynamics - Equilibrium Phase-Space Distributions. *Phys. Rev. A*, 31(3), 1695–1697. <https://doi.org/10.1103/PhysRevA.31.1695>

Hsu, S. M. (2004). Nano-lubrication: Concept and design. *Tribology International*, 37(7), 537–545. <https://doi.org/10.1016/j.triboint.2003.12.002>

Jorgensen, W. L., & Swenson, C. J. (1984). Optimized Intermolecular Potential Functions for Liquid Hydrocarbons. *Journal of the American Chemical Society*, 106(3), 6638–6646.

<https://doi.org/10.1021/ja00289a008>

Khare, R., Keblinski, P., & Yethiraj, A. (2006). Molecular dynamics simulations of heat and momentum transfer at a solid-fluid interface: Relationship between thermal and velocity slip. *International Journal of Heat and Mass Transfer*, 49(19–20), 3401–3407. <https://doi.org/10.1016/j.ijheatmasstransfer.2006.03.005>

Ko, F. K. (1985). *FRICITION AND WEAR OF POLYMER COMPOSITES*.

Landry, E. S., & Mcgaughey, A. J. H. (2009). *Thermal boundary resistance predictions from molecular dynamics simulations and theoretical calculations*. 1–26.

Leimkuhler, B., Reich, S., & Skeel, R. (1996). Integration methods for molecular dynamics. *Mathematical Approaches to Biomolecular Structure and Dynamics*, 161–185. https://doi.org/10.1007/978-1-4612-4066-2_10

Li, X., & Yang, R. (2012). Effect of lattice mismatch on phonon transmission and interface thermal conductance across dissimilar material interfaces. *Physical Review B - Condensed Matter and Materials Physics*, 86(5). <https://doi.org/10.1103/PhysRevB.86.054305>

Lincoln, R. C., Koliwad, K. M., & Ghate, P. B. (1967). Morse-potential evaluation of second- and third-order elastic constants of some cubic metals. *Physical Review*, 157(3), 463–466. <https://doi.org/10.1103/PhysRev.157.463>

Marcus G. Martin and J. Ilja Siepmann. (1998). Transferable Potentials for Phase Equilibria. 1. United-Atom Description of n-Alkanes. *The Journal of Physical Chemistry B*, 102(25), 2569–2577.

Mondello, M., & Grest, G. S. (1995). Molecular dynamics of linear and branched alkanes. *The Journal of Chemical Physics*, 103(16), 7156–7165. <https://doi.org/10.1063/1.470344>

Morse Philip M. (1929). Diatomic molecules according to the wave mechanics. II. vibrational levels. *Physical Review*, 34(1), 57–64.

Nose, S. (2002). A molecular dynamics method for simulations in the canonical ensemble. *Molecular Physics*, 100(1), 191–198. <https://doi.org/10.1080/00268970110089108>

Nose, Shuichi. (1984). A unified formulation of the constant temperature molecular

dynamics methods. *The Journal of Chemical Physics*, 81(1), 511–519.
<https://doi.org/10.1063/1.447334>

Nose, Shuichi. (1991). *Constant Temperature Molecular Dynamics Methods*.

Ohara, T., & Suzuki, D. (2000). Intermolecular energy transfer at a solid-liquid interface. *Microscale Thermophysical Engineering*, 4(3), 189–196.
<https://doi.org/10.1080/10893950050148142>

Ohara, Taku. (1999a). Contribution of intermolecular energy transfer to heat conduction in a simple liquid. *Journal of Chemical Physics*, 111(21), 9667–9672.
<https://doi.org/10.1063/1.480338>

Ohara, Taku. (1999b). Intermolecular energy transfer in liquid water and its contribution to heat conduction: A molecular dynamics study. *Journal of Chemical Physics*, 111(14), 6492–6500. <https://doi.org/10.1063/1.480025>

Ohara, Taku, & Torii, D. (2005). Molecular dynamics study of thermal phenomena in an ultrathin liquid film sheared between solid surfaces: The influence of the crystal plane on energy and momentum transfer at solid-liquid interfaces. *Journal of Chemical Physics*, 122(21). <https://doi.org/10.1063/1.1902950>

Ohara, Taku, Yuan, T. C., Torii, D., Kikugawa, G., & Kosugi, N. (2011). Heat conduction in chain polymer liquids: Molecular dynamics study on the contributions of inter- and intramolecular energy transfer. *Journal of Chemical Physics*, 135(3). <https://doi.org/10.1063/1.3613648>

Park, S. J., & Seo, M. K. (2011). Solid-Liquid Interface. In *Interface Science and Technology* (Vol. 18). <https://doi.org/10.1016/B978-0-12-375049-5.00003-7>

Parrinello, M., & Rahman, A. (1981). Polymorphic transitions in single crystals: A new molecular dynamics method. *Journal of Applied Physics*, 52(12), 7182–7190.
<https://doi.org/10.1063/1.328693>

Rafeq, A., Saleman, B., Munir, F. A., Fadzli, M., Abdollah, B., Kikugawa, G., & Ohara, T. (2018). *Comparison of the characteristic of heat transport between non-shear and shear systems at solid-liquid (S-L) interfaces*. (May), 270–272.

Ruhle, V. (2008). Pressure coupling/barostats. *Journal Club Handout*, (3), 1–5. <https://doi.org/10.1016/B978-0-08-021161-9.50006-2>

Saleman, A.R., Munir, F. A., Zin, M. R. M., Yob, M. S., Kikugawa, G., & Ohara, T. (2018). Heat transport at solid-liquid interfaces between face-centered cubic lattice and liquid alkanes. *Journal of Advanced Research in Fluid Mechanics and Thermal Sciences*, 44(1), 123–130.

Saleman, Abdul Rafeq bin, Chilukoti, H. K., Kikugawa, G., Shibahara, M., & Ohara, T. (2017a). A molecular dynamics study on the thermal energy transfer and momentum transfer at the solid-liquid interfaces between gold and sheared liquid alkanes. *International Journal of Thermal Sciences*, 120, 273–288. <https://doi.org/10.1016/j.ijthermalsci.2017.06.014>

Saleman, Abdul Rafeq bin, Chilukoti, H. K., Kikugawa, G., Shibahara, M., & Ohara, T. (2017b). A molecular dynamics study on the thermal transport properties and the structure of the solid-liquid interfaces between face centered cubic (FCC) crystal planes of gold in contact with linear alkane liquids. *International Journal of Heat and Mass Transfer*, 105, 168–179. <https://doi.org/10.1016/j.ijheatmasstransfer.2016.09.069>

Soong, C. Y., Yen, T. H., & Tzeng, P. Y. (2007). Molecular dynamics simulation of nanochannel flows with effects of wall lattice-fluid interactions. *Physical Review E - Statistical, Nonlinear, and Soft Matter Physics*, 76(3), 1–14. <https://doi.org/10.1103/PhysRevE.76.036303>

Streator, J. L. (2015). *Solid-Liquid-Solid Interfaces*.

Stuart, S. J., Zhou, R., & Berne, B. J. (1996). Molecular dynamics with multiple time scales: The selection of efficient reference system propagators. *American Institute of Physics*, 105(4), 1426–1436.

Swartz, E. T., & Pohl, R. O. (1989). Thermal boundary resistance. *Reviews of Modern Physics*, 61(3), 605–668. <https://doi.org/10.1103/RevModPhys.61.605>

Tildesley, M. P. A. J. (n.d.). *Allen-Tildesley computer simulation of Liquids.pdf*.

Torii, D., Nakano, T., & Ohara, T. (2008). Contribution of inter- and intramolecular energy transfers to heat conduction in liquids. *Journal of Chemical Physics*, 128(4), 1–9. <https://doi.org/10.1063/1.2821963>

Torii, D., & Ohara, T. (2007). Molecular dynamics study on ultrathin liquid water film sheared between platinum solid walls: Liquid structure and energy and momentum transfer. *Journal of Chemical Physics*, 126(15). <https://doi.org/10.1063/1.2719699>

Torii, D., Ohara, T., & Ishida, K. (2010). Molecular-Scale Mechanism of Thermal Resistance at the Solid-Liquid Interfaces: Influence of Interaction Parameters Between Solid and Liquid Molecules. *Journal of Heat Transfer*, 132(1), 012402. <https://doi.org/10.1115/1.3211856>

Torii, D., Taku Ohara, & Kenji Ishida. (2007). MOLECULAR SCALE MECHANISM OF THERMAL RESISTANCE AT SOLID-LIQUID INTERFACES (INFLUENCE OF INTERACTION PARAMETERS BETWEEN SOLID AND LIQUID MOLECULES). *Thermal Engineering*, 1–9.

Ungerer, P., Beauvais, C., Delhommelle, J., Boutin, A., Rousseau, B., & Fuchs, A. H. (2000). Optimization of the anisotropic united atoms intermolecular potential for n-alkanes. *Journal of Chemical Physics*, 112(12), 5499–5510. <https://doi.org/10.1063/1.481116>

Wm.G.Hoover, C. G. H. (2005). Non-equilibrium molecular dynamics. *Handbook of Materials Modeling*, 8(2), 745–761. <https://doi.org/10.1063/1.1900484>

Woodcock, L. V. (1971). ISOTHERMAL MOLECULAR DYNAMICS CALCULATIONS FOR LIQUID SALTS. *Chemical Physics Letters*, 10(3). [https://doi.org/org/10.1016/0009-2614\(71\)80281-6](https://doi.org/org/10.1016/0009-2614(71)80281-6)

Yang, J. Z., Wu, X., & Li, X. (2012). A generalized Irving-Kirkwood formula for the calculation of stress in molecular dynamics models. *Journal of Chemical Physics*, 137(13). <https://doi.org/10.1063/1.4755946>

Zhang, J., & Todd, B. D. (2004). *Pressure tensor and heat flux vector for inhomogeneous nonequilibrium fluids under the influence of three-body forces*. 1–11.

<https://doi.org/10.1103/PhysRevE.69.031111>

Zhang, M., & Skeel, R. D. (1997). Cheap implicit symplectic integrators. *Applied Numerical Mathematics*, 25(2–3), 297–302. [https://doi.org/10.1016/S0168-9274\(97\)00066-4](https://doi.org/10.1016/S0168-9274(97)00066-4)

Zhigilei, L. (2013). Introduction to interatomic potentials (I). *None*, (I).



APPENDICES

The study was conducted to as follows:-

Table 1.1: Gantt chart of PSM 1 for this study.

Task	PSM 1			
	September	October	November	December
PROJECT INTRODUCTION * Problem Statement * Objectives * Scope	■			
REVIEW LITERATURE WORK * Review literature (Journal and book) * Findings additional information and knowledge about project		■		
METHODOLOGY * Simulation work * Prediction result			■	
PRELIMINARY RESULT * Result From Simulation			■	
PRESENTATION PSM 1 * Mooc Presentation * Complete PSM 1 Report				■

اونيورسيتي تيكنيكل مليسيا ملاك

Table 1.2: Gantt chart of PSM 2 for this study.

Task	PSM 2			
	February	March	April	May
SIMULATION PROCESS * Non-shear setup * Shear setup * Compile result	■			
ANALYZE AND DISCUSSION * Analyze data collection * Discussion			■	
PREPARATION AND PRESENTATION FINAL REPORT * Make conclusion, complete the final report and presentation			■	